PUBLICATIONS OF
THE UNIVERSITY OF EASTERN FINLAND

Dissertations in Forestry and Natural Sciences

PIA PUHAKKA

OPTICAL COHERENCE TOMOGRAPHY OF ARTICULAR CARTILAGE

Towards Quantitative Arthroscopic Applications

PIA PUHAKKA

Optical Coherence Tomography of Articular Cartilage

Towards Quantitative Arthroscopic Applications

Publications of the University of Eastern Finland
Dissertations in Forestry and Natural Sciences
No 212

Academic Dissertation
To be presented by permission of the Faculty of Science and Forestry for public examination in the Auditorium SN201 in Snellmania Building at the University of Eastern Finland, Kuopio, on January, 30, 2016,
at 12 o'clock noon.

Department of Applied Physics

Grano Oy
Jyväskylä, 2016
Editors: Prof. Pertti Pasanen, Prof. Kai Peiponen,
Prof. Pekka Kilpeläinen, Prof. Matti Vornanen

Distribution:
University of Eastern Finland Library / Sales of publications
P.O. Box 107, FI-80101 Joensuu, Finland
tel. +358-50-3058396
http://www.uef.fi/kirjasto

ISBN: 978-952-61-2019-5 (printed)
ISSNL: 1798-5668
ISSN: 1798-5668
ISBN: 978-952-61-2020-1 (pdf)
ISSNL: 1798-5668
ISSN: 1798-5676

Author's address:
University of Eastern Finland
Department of Applied Physics
P.O.Box 1627
70211 KUOPIO
FINLAND
email: pia.puhakka@uef.fi

Supervisors:
Professor Juha Töyräs, Ph.D.
University of Eastern Finland
Department of Applied Physics
Kuopio, FINLAND
email: juha.toyras@uef.fi

Dean, Professor Jukka Jurvelin, Ph.D.
University of Eastern Finland
Department of Applied Physics
Kuopio, FINLAND
email: jukka.jurvelin@uef.fi

Tuomas Virén, Ph.D.
Kuopio University Hospital
Cancer Center
Kuopio, FINLAND
email: tuomas.viren@kuh.fi

Reviewers:
Professor Valery Tuchin, Ph.D.
Saratov State University
Research-Educational Institute of Optics and Biophotonics
83 Astrakhanskaya street
410012 Saratov
RUSSIA
email: tuchinvv@mail.ru

Associate Professor Travis Klein, Ph.D.
Queensland University of Technology
Institute of Health and Biomedical Innovation
60 Musk Ave
Kelvin Grove Qld 4059
AUSTRALIA
email: t2.klein@qut.edu.au

Opponent:

Professor Antonius van Leeuwen, Ph.D.
Academic Medical Center
Biomedical Engineering and Physics
Amsterdam
NETHERLANDS

ABSTRACT

Osteoarthritis (OA) is a common joint disease causing joint dysfunction and pain. At present, there is no cure for OA, but several surgical techniques have been developed which can prevent, or at least slow down, the progression of the disease. It would be important if clinicians could make an accurate diagnosis of the severity and extent of an articular cartilage lesion since this would allow selection of the optimal treatment method. Moreover, *in vivo* monitoring of native articular cartilage or cartilage repair tissue properties, like thickness, structure and morphology would be valuable in the development of new treatment methods. Optical coherence tomography (OCT) can be used to obtain high resolution cross-sectional images of articular cartilage without any need to damage the tissue. Furthermore, OCT imaging can be applied during an arthroscopic examination, although this technique has not yet entered into routine clinical use.

This thesis evaluated the feasibility of arthroscopic OCT. The applicability of OCT imaging in arthroscopy was first tested in multiple human cadaver joints. Next, the sensitivity of OCT to detect changes in the collagen and chondrocyte contents in agarose scaffolds and its capability to observe the characteristics of articular cartilage were investigated via the measurement of light attenuation and backscattering coefficients. Furthermore, partial least squares (PLS) regression models were developed for the estimation of structural, compositional and biomechanical properties of articular cartilage from the depth dependent OCT signal. The accuracy of determination of cartilage thickness from OCT images was investigated. The thickness measurement was further applied with simultaneous ultrasound imaging to determine the speed of sound (SOS) in articular cartilage, a property which is known to decrease as cartilage degenerates. Finally, OCT imaging was applied *in vivo* to assess the success of cartilage repair conducted in equine stifle joint.

OCT was found to be applicable for arthroscopic imaging of

articular cartilage in multiple human joints. The light attenuation coefficient measured using OCT correlated significantly ($p < 0.05$) with both the collagen and chondrocyte contents of the agarose scaffolds, whereas PLS analysis of depth-dependent OCT signal was found to be promising in the prediction of collagen orientation, permeability, proteoglycan content and histological integrity of equine cartilage. With OCT, it was possible to perform an accurate thickness measurement of equine non-calcified and full cartilage layers. Thickness measurement was proven also to be feasible in the arthroscopy of human joints, in locations with cartilage thickness less than the light penetration depth. Combined OCT and ultrasound imaging for determination of SOS in cartilage was assessed as promising, although at present, it is not a sufficiently accurate technique to permit the arthroscopic evaluation of the degenerative stage of cartilage. In cartilage surgical procedures, OCT was found to be beneficial when estimating the thickness and structure of the repair tissue as well as the filling of the defect.

To conclude, arthroscopic OCT imaging, as a complementary technique to conventional arthroscopy, holds the potential to allow both the qualitative and quantitative evaluation of articular cartilage. It is concluded that after optimization of the imaging geometry and further validation, the quantitative characterization of articular cartilage with arthroscopic OCT may well proceed to routine clinical use.

National Library of Medicine Classification: QT 36, WE 300, WE 348, WN 206

Medical Subject Headings: Diagnostic Imaging; Tomography, Optical Coherence; Joints; Cartilage, Articular; Osteoarthritis; Wounds and Injuries; Arthroscopy/methods

Yleinen suomalainen asiasanasto: kuvantaminen; optinen koherenssitomografia; sironta; nivelet; nivelrusto; nivelrikko; vammat; tähystysleikkaukset

Preface

This study was carried out during the years 2011-2015 in the Department of Applied Physics, University of Eastern Finland and Kuopio University Hospital.

I thank my supervisors Professor Juha Töyräs, Dean Jukka Jurvelin, and Tuomas Virén, Ph.D., for giving me the opportunity to join the Biophysics of Bone and Cartilage research group, and the guidance throughout the project. I am most grateful to Juha whose diligence, energy, and ideas drove also my thesis to the finish line. Jukka's experience, calmness and wider perspective as well as the practical instructions from Tuomas were essential while working on the studies. Moreover, the studies could have not been completed without the contribution of all the co-authors.

I want to express my sincere thanks to the official reviewers of this thesis, Professor Valery Tuchin, Ph.D., and Associate Professor Travis Klein, Ph.D., for their professional review and constructive criticism. Moreover, I want to thank Ewen MacDonald, D.Pharm., for linguistic review.

The colleagues Jari Rautiainen, Satu Inkinen, Jukka Liukkonen, Chibuzor Eneh, Juuso Honkanen, Markus Malo, Kimmo Halonen, Nikae te Moller and the others; it has been a great time! It means a lot to have a group like this for support and to have fun with.

Outside the office, Maiju and the rest of the HMG made Kuopio feel like a second home. I feel sorry, that I have not found time to join the games lately.

I am grateful for all the encouragement and love given by my family; my mother Jaana, and Hannu, Mari and Saku. They have practically taught me everything I know. My beloved Hans, of the outcomes of all the time spent in the lab, you are definitely the best.

This study was financially supported by Jenny and Antti Wihuri Foundation, Kuopio University Hospital, Academy of Finland, and National Doctoral Programme of Musculoskeletal Disorders and Biomaterials, which I acknowledge with gratitude.

Kuopio, January 2016

Pia Puhakka

ABBREVIATIONS

ABS	acrylonitrile butadiene styrene
AU	arbitrary unit
CCD	charge-coupled device
CECT	contrast-enhanced computed tomography
CT	computed tomography
CVrms(%)	percentual root mean square coefficient of variation
DJD	Degenerative Joint Disease
EDTA	ethylenediaminetetraacetic acid
FD-OCT	Fourier domain optical coherence tomography
FE	finite element
FTIR	Fourier transform infrared spectroscopy
FWHM	full-width-at-half-maximum
GelMA	gelatin methacrylamide
ICC	intra-class correlation coefficient
ICRS	International Cartilage Repair Society
MC3	dorsoproximal areas of the third metacarpal bone
MCP1	first metacarpophalangeal joint
MRI	magnetic resonance imaging
MTP1	first metatarsophalangeal joint
NA	numerical aperture
OA	osteoarthritis
OD	optical density
OCT	optical coherence tomography
P1	proximal phalanx
PBS	phosphate-buffered saline
PCL	polycarpolactone
PG	proteoglycan
PI	parallelism index
PLS	partial least squares
PS-OCT	polarization sensitive optical coherence tomography
RMSECV	root mean square error in cross-validation
RMSEP	root mean square error in prediction
ROI	region of interest

SD	standard deviation
SD-OCT	spectral domain optical coherence tomography
SOS	speed of sound
SR	sagittal ridge
SS-OCT	swept source optical coherence tomography
T2	transverse relaxation time
TOF	time-of-flight
US	ultrasound

SYMBOLS AND NOTATIONS

$b(d)$	depth-dependent optical coherence tomography signal
c	speed of light
d	probing depth
d_0	focus position
E_f	fibril network modulus
E_m	non-fibrillar matrix modulus
E_r	electric field returning from the reference arm
E_s	electric field returning from the sample arm
f_0	center frequency
f_D	Doppler shift
I_{0°	light intensity in background corrected 0° image
I_{45°	light intensity in background corrected 45° image
I_{90°	light intensity in background corrected 90° image
$I_{90^\circ+\lambda/4}$	light intensity in background corrected 90° image taken with $\lambda/4$ phase shifter
I_D	intensity of light at the detector
I_{max}	maximum intensity
I_{min}	minimum intensity
I_r	intensity of light returning from the reference arm
I_s	intensity of light returning from the sample arm
k	permeability
L_c	coherence length
$L_{c,medium}$	coherence length in medium
n_i	group refractive index of medium i
N	number of samples
N_{comp}	number of components in partial least squares regression model
p	level of statistical significance
R^2	coefficient of determination
S_0	total light intensity
S_1	intensity of light with linear horizontal or vertical polarization
S_2	intensity of light with linear +45° or -45° polarization
S_3	intensity of light with circular polarization

t	time
y	predicted response variable value
$\widehat{y}$	true response variable value
z_0	apparent Rayleigh length
δx	lateral resolution
$\Delta\lambda$	wavelength range
ΔL	optical path length difference
γ_{sr}	degree of the coherence
λ_0	central wavelength
μ_b	backscattering coefficient
μ_t	total attenuation coefficient
π	pi
ρ	Spearman's rank correlation coefficient
τ	time delay
Ψ	orientation angle of polarization ellipse
$\|\ldots\|$	absolute value
$<>$	time average
*	complex conjugate

LIST OF PUBLICATIONS

This thesis consists of the present review of the author's work related to the field of optical coherence tomography of articular cartilage and the following selection of the author's publications:

I Puhakka PH, Ylärinne J, Lammi M, Saarakkala S, Tiitu V, Kröger H, Virén T, Jurvelin JS, Töyräs J, "Dependence of light attenuation and backscattering on collagen and chondrocyte density in agarose scaffolds," *Physics in Medicine and Biology* **59**: 6537-6548, 2014

II Puhakka PH, te Moller NCR, Afara IO, Mäkelä JTA, Tiitu V, Korhonen RK, Brommer H, Virén T, Jurvelin JS, Töyräs J, "Estimation of articular cartilage properties using multivariate analysis of optical coherence tomography signal," *Osteoarthritis and Cartilage* **23**: 2206-2213, 2015

III Puhakka PH, te Moller NCR, Tanska P, Saarakkala S, Tiitu V, Korhonen RK, Brommer H, Virén T, Jurvelin JS, Töyräs J, "Optical coherence tomography enables accurate equine cartilage thickness measurement for determination of speed of sound," *Submitted, 2015*

Throughout the thesis, these papers are referred to by Roman numerals.

The thesis also contains previously unpublished data, which are referred to in the text as **A** and **B**.

AUTHOR'S CONTRIBUTION

The publications selected in this dissertation are original research papers on optical coherence tomography. The author was involved in the planning and design of each study. In all publications, the author has conducted or supervised the optical coherence tomography measurements and carried out all data analyses. In addition, the author conducted the reference analyses in study **I**. The author has written the manuscripts for papers **I-III**. In all papers the collaboration with the co-authors has been significant.

In unpublished studies **A** and **B**, the author contributed to the design of the studies, supervised and assisted in OCT, ultrasound and arthroscopic imaging conducted by physicians, and analyzed the image data.

Contents

1 Introduction

Articular cartilage is a thin layer of soft tissue covering the ends of articulating bones. During movement, articular cartilage and synovial fluid provide low friction between the bones, preventing wear of the articulating surfaces [1,2]. Another role of articular cartilage is to, act together with the menisci to absorb the mechanical energy during movement and distribute the loads to which the joints are exposed [3,4].

The main components of articular cartilage are water, collagen, proteoglycans and chondrocytes, which all have specific roles in the function of the tissue [1]. Water, collagen network, and proteoglycans contribute to the mechanical properties of articular cartilage, whereas chondrocytes maintain the tissue by synthesizing and organizing its components.

Osteoarthritis (OA) is a disease causing a gradual degeneration of articular cartilage. In early stage of OA, the amount of proteoglycans in cartilage decreases, the collagen matrix becomes disrupted and there are also changes in the chondrocyte content. The tissue becomes softened due to disruption of the collagen network and loss of proteoglycans, and becomes prone to wear and tear [5]. Although the underlying cause of OA is usually unknown, the prevalence of OA increases substantially with aging and if the subject is obese [5–7]. Usually, degeneration occurs when natural repair of cartilage is disturbed. Sometimes, the development of OA is initiated by a focal mechanical cartilage injury. In this case, the disease is referred to as post-traumatic OA [5,8,9].

Injuries, OA, and the pain they cause are mainly treated with pharmacological pain relief or by surgical procedures [10]. However, novel treatment options are being actively developed. The choice of the surgical treatment method is made partly based on the location, size, depth and shape of the lesion, as well as the extent of the cartilage degeneration [10,11]. Nevertheless, the abil-

ity to assess the severity of cartilage injuries and early stage OA is limited [12]. Injuries are usually first diagnosed in a clinical investigation, possibly followed by radiography, computed tomography (CT), or magnetic resonance imaging (MRI) [12]. Unfortunately these diagnostic methods lack sensitivity to detect minor cartilage injuries. Cartilage is not visible in radiographic images [13], and the limited resolution of current CT and MRI devices means that the detection of small and early stage changes is rather problematic with these modalities [14–17]. The condition of cartilage can also be evaluated arthroscopically during meniscus, ligament or some other type of joint repair surgery. In an arthroscopic examination, the severity of the detected lesion is evaluated based on a visual assessment and palpation. However, conventional arthroscopy may not be optimal in the detection of early stage tissue changes or in the estimation of the severity and size of the lesion since only surface of the tissue can be visualized. The evaluation of cartilage lesions and degeneration of the articulating surfaces based on arthroscopic image is subjective, poorly repeatable and it has been considered by experts to be inaccurate [18–20].

Optical coherence tomography (OCT) has been proposed as a tool for quantitative assessment of the degenerative state of articular cartilage. Due to the high resolution (3-20 µm) of this imaging technique, it is possible to determine accurately both the cartilage lesion type and size [21, 22]. Furthermore, light attenuation, backscattering, and changes in collagen fibril orientation in soft tissue can be quantified using OCT [23–25]. OCT imaging has already been applied during arthroscopy, but the technique is currently not in routine clinical use [26].

This thesis further examines the feasibility of OCT imaging in arthroscopic procedures. The feasibility of using a small OCT probe for arthroscopic imaging of human shoulder, elbow, wrist, knee, ankle and first metacarpo- and metatarsophalangeal joints was tested *in situ*. The same probe type was further used to investigate the potential usefulness of quantitative analysis of cartilage OCT images. First, the effect of cartilage components, *i.e.* chondrocytes

and collagen, on near-infrared light attenuation and backscattering was studied using agarose gel scaffolds with varying chondrocyte or collagen contents. Next, the ability to estimate compositional, structural, and biomechanical properties of equine cartilage from the OCT signal was investigated *in vitro*. Furthermore, the accuracy of OCT-based measurement of equine non-calcified and calcified cartilage thickness was studied *in vitro*. In addition, a technique combining OCT and ultrasound imaging for arthroscopic measurement of the speed of sound (SOS) in cartilage, a sensitive index of cartilage integrity, was introduced and assessed. Finally, the arthroscopic OCT imaging was used in the *in vivo* evaluation of cartilage repair surgery conducted in equine stifle joints and for evaluation of healing after a surgical intervention.

2 Articular cartilage and osteoarthritis

Articular cartilage present in the articulating ends of bones plays a significant role in smooth movement of the joints, and absorption and distribution of the mechanical energy during movement. This connective tissue has a unique structure and composition formed by solid matrix and interstitial fluid. Articular cartilage has no innervation. Therefore, minor wear and tear and even small injuries in cartilage may be asymptomatic. Due to the lack of vascular system the tissue has a poor regeneration ability, such that with the passage of time, these small injuries and minor disruption may lead to more severe and often symptomatic damage to the articular cartilage.

2.1 STRUCTURE OF ARTICULAR CARTILAGE

Articular cartilage is mainly composed of water, collagen fibrils, proteoglycans and the chondrocytes. About 60-85% of the tissue is water, whereas 50-80% of the tissue dry weight is collagen [1]. Most of the collagen is of type II and the fibril diameter varies between 20 and 200 nm [1, 27]. Proteoglycans account for about 25-35% of cartilage dry weight. Chondrocytes contribute less than 5% of cartilage volume. The highly specialized chondrocytes synthesize and maintain articular cartilage and organize the collagens and proteoglycans into a specific structure [1, 27].

Based on the orientation of collagen fibrils, articular cartilage can be divided into three zones. The layer of calcified cartilage located between the non-calcified cartilage and subchondral bone can be considered as a fourth zone (Figure 2.1) [27]. In the superficial zone (the first 5-20% of cartilage thickness), collagen fibrils are mostly oriented in parallel to the cartilage surface [28]. This parallel orientation of the collagen provides the cartilage surface with good

strength and tensile stiffness, conferring a high resistance against shear forces [27]. The superficial zone has a higher collagen content and a lower proteoglycan content than the other zones [1]. In the superficial zone, the chondrocytes are ellipsoid in shape [3]. In the middle or transitional zone (5-20% of cartilage thickness [28]), collagen orientation is more random. Here, the chondrocytes are spheroidal and the collagen fibrils have a higher diameter [27]. In the deep zone (60-90% of cartilage thickness [28]), collagen fibrils are oriented perpendicular to the cartilage surface and they have a larger diameter than in the other zones. Chondrocytes tend to align in columns and the proteoglycan content is higher than that in the superficial and middle zones [1]. A layer of calcified cartilage separates cartilage and subchondral bone. Here, the chondrocytes have a smaller volume [27]. Collagen fibers from the deep zone run through the calcified zone and are attached to the subchondral bone. The tidemark lies between the non-calcified and calcified layers; this is a line seen in microscopic images due to its basophilic nature [27].

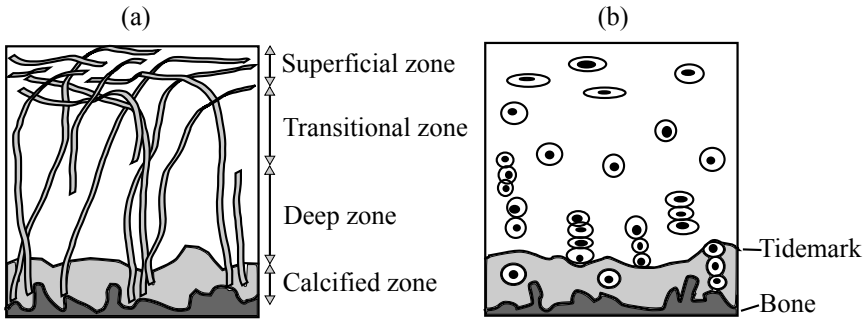

Figure 2.1: Schematic illustration of the structure of articular cartilage. (a) In the superficial zone, collagen fibrils are highly organized in parallel to the cartilage surface. In the transitional zone, collagen orientation is more random as the fibrils slowly begin to align perpendicular to the surface. In the deep zone, the fibrils take on a perpendicular orientation. Collagen fibrils penetrate through the calcified zone and attach to subchondral bone. (b) Chondrocytes of cartilage superficial zone are ellipsoid in shape. In the middle zone, they are more spheroidal and towards the deep zone, they are aligned into columns.

The ability of articular cartilage to mechanically adapt to high and low forces is promoted by water, since this can move within the tissue. Proteoglycans have a negative charge which attracts water molecules. The difference in the concentration of ions between cartilage and synovial fluid means that there is a high osmotic swelling pressure in the tissue. However, the swelling is resisted by the collagen network. Cartilage has a relatively low permeability, which is partially regulated by proteoglycans. During high rate loading such as in jumping, the fluid flow within the tissue is restricted by the low permeability. The pressure inside the tissue increases, as water cannot leave the tissue. The high pressure and the collagen network restrict the shape deformation of cartilage and the tissue acts almost like incompressible material. During static loading, *i.e.* when standing, water has time to flow slowly within and out of cartilage, which enables tissue deformation and an adaptation to the force. When the loading ends, water flows back into the tissue [1,4,29].

2.2 OSTEOARTHRITIS

With time, the stresses and strains experienced by articular cartilage may lead to small, micron-scale cracks appearing on articular cartilage surface [1]. OA occurs when the tissue fails to generate new cartilage to replace the damaged tissue. The small cracks may then further grow to become visually observable damage. OA differs from normal aging, although they share some similar features at tissue level [5].

In the first stage of OA, there is a loss of large aggregating proteoglycans and the collagen network becomes disrupted [5,27]. In particular, disruption of the superficial zone increases the permeability of cartilage, resulting in a lower tensile stiffness of the tissue. In this way, cartilage becomes vulnerable to subsequent damage [27]. The first visible sign of OA is fibrillation of the cartilage surface. This may occur in the first or second stage of the disease [3]. In the second stage, chondrocytes respond to the degener-

ation by attempting to clear the damaged components, speed up the syntheses of both collagen and proteoglycan and promote cell proliferation [5]. When the chondrocyte response fails to prevent the degeneration, the disease progresses to the third stage. The chondrocyte metabolism decelerates and cartilage is lost progressively due to further loss of proteoglycans and fibrillation of the cartilage surface. Finally, cartilage is completely lost and the underlying subchondral bone becomes exposed.

Osteoarthritic changes are not limited only to cartilage tissue, but the disease affects the whole joint. Remodeling of the subchondral bone usually occurs during the development of OA. The volume and density of subchondral bone increase and cyst-like bone cavities and osteophytes may be formed. The disease usually affects also synovial membrane, ligaments, and the muscles acting across the joint [3].

Joint injuries, *e.g.* ligament or meniscus tears, or cartilage injuries may initiate or accelerate the development of OA [30]. In the case of injury-initiated OA, the disease is called as post-traumatic OA. Cartilage damage may follow from an acute joint injury even though no signs of visible damage are seen [12, 31]. The repair and healing potential of the tissue depends on the energy of the impact causing the injury [30]. In addition, the severity of the damage depends on the orientation and rate of the loading. In simple terms, lighter impacts cause cell damage and cell death, disruption of cartilage macromolecular framework, proteoglycan loss, and an increase in the water concentration, whereas stronger impacts may also cause superficial fissures or even fractures extending to bone [8, 30]. All of these alter the mechanical function of cartilage and make the tissue prone to further damage. However, the biological factors behind the development of post-traumatic OA are not well known [8].

The main symptoms of cartilage degeneration are pain and swelling, stiffness, and limited movement of the joint [5]. OA is most frequently encountered in the hand, knee, and hip joints. Among adult population (age $\geq$ 26 years), the prevalence of radio-

graphic OA in hand and hip joints have been reported to be 27.2% and 13.8%, respectively [6]. Frequently, OA leads to a reduced quality of life and incapacity for work, and thus it poses a significant economic burden on both the individual sufferer and the society. Almost 5% of the people between ages 15 and 44, between 25-30% of 45-64 year-olds and to the vast majority, 90%, of people over 65 years of age have some level of OA [3]. Severe knee OA has been found in 1% of 25-34 year-olds and in 30% of people over 75 years of age [32]. Moreover, about 10% of people over 55 years have been reported to suffer from a painful and disabling knee OA [33]. In particular, the prevalence of OA is high among persons subjected to repetitive and excessive type of joint use and high impacts due to physically demanding work, sport, or obesity [4].

2.2.1 Treatment

With current treatment methods, it is not possible to fully stop the progression of OA. However, the symptoms can be treated and in some cases the progression can be slowed down. OA and cartilage injuries are treated non-surgically with pain-relieving and anti-inflammatory medication, corticosteroid injections, viscosupplementation, physiotherapy, heat and cold treatment, bracing and orthotics, weight reduction and changing the activity level [34–38]. Additionally, surgical treatment methods have been developed for repairing the cartilage damage [39].

Total joint replacement is the most widely used surgical treatment for older people with severe and disabling OA. In the United States, about 350 000 knee and hip replacements are performed annually [32]. This involves a major surgical operation and it may not optimal for young patients as the endoprostheses have limited lifetimes.Young people suffering from cartilage injury and at the risk of developing post-traumatic OA may benefit from alternative surgical treatment methods like stimulation of the repair mechanisms of cartilage, or replacement of the damaged cartilage with osteochondral transplants or engineered repair tissue [40–42].

The repair mechanisms of cartilage can be stimulated with sur-

gical techniques. One widely used technique is microfracturing, in which the subchondral plate is perforated in order to cause hemorrhage and allow the migration of mesenchymal stem cells into the defect [43]. Typically, cartilage responds to this stimulation by creating fibrocartilage tissue, which unfortunately, has reduced resilience and stiffness compared to hyaline cartilage [10].

Chondrocytes can be transplanted into the cartilage defect; in this case, the healing response involves the growth of hyaline cartilage rather than fibrocartilage [44]. In autologous chondrocyte implantation, the chondrocytes are first isolated from tissue, which is harvested from a less weight bearing area and the cells are cultured. In a second operation, the chondrocytes are injected into the lesion and covered with a periosteal graft. Allogenic chondrocytes can also be used [45].

In osteochondral transplantation, the damaged cartilage area is resurfaced with an osteochondral autograft or allograft. The autologous transplants are obtained from the less weight bearing area of the articulating surface and the allograft from a cadaveric donor. The success of the transplantation depends on how well the transplant integrates with the surrounding cartilage and the healing of the donor site, if autologous transplants are used [46]. In allograft transplantation, the healing of the donor site is not an issue, but transplant incorporation is slower [47].

A promising and relatively new approach is to use tissue-engineered matrices in place of the ostechondral transplants [48, 49]. Often the tissue-engineered implants are formed from a scaffold material in which chondrocytes and stem cells are embedded. The cells are expected to generate a new extracellular matrix with or without stimulation [42]. The scaffold needs to be biocompatible, natural or synthetic and preferably a biodegradable material that becomes fixed well to the defect site. It should allow cell migration and adhesion, and be mechanically durable [50]. Many studies have already been conducted and and even more are in progress to optimize of the properties and manufacturing process of the engineered tissue [51–53].

In summary, the range of non-operative and operative treatment methods is wide and new methods are developing all the time. Even though the prognosis for the healing is unclear, early diagnosis and treatment improve the outcome. The treatment method is usually chosen based on the patient's age and the type, location, size, depth, and severity of the lesion and condition of the cartilage surrounding the lesion [10]. Thus, it is clearly important to have the capability to diagnose cartilage injuries and OA as early as possible, and to be able to measure the defect size and health of the surrounding tissue prior to repair surgery. Furthermore, when developing new operative and non-operative treatment methods, it would also be advantageous to be able to quantitatively and accurately follow the success of the repair or progression of the osteoarthritic degeneration.

2.2.2 Diagnostics

OA and cartilage injuries are usually diagnosed based on the symptoms of the patient, anamnesis, and radiographic images. Malalignment of the joint is a contributing factor for OA, but it can also be a symptom. The other main symptoms are pain, swelling and locking of the joint, symptoms which can be diagnosed by a general practitioner [3]. The OA diagnosis made from a radiographic image is based on detection of osteophyte formation and joint space narrowing, which is clearly visible due to cartilage loss [54]. However, cartilage injuries and early stage OA cannot be detected with radiography as cartilage is not visible in conventional radiographic images.

Computed tomography (CT) is a more advanced radiographic technique. Contrast enhanced CT (CECT) imaging enables visualization of articular cartilage as the contrast agent absorbs X-rays and therefore enhances the contrast in the target tissue [55]. Currently, negatively charged contrast agents are used in cartilage imaging. The amount of anionic contrast agent diffusing into the cartilage is inversely proportional to the content of the negatively charged proteoglycans in cartilage [55]. Additionally, mechanical injuries

may increase the permeability and therefore the uptake of the contrast agent [56]. Thus, the trauma or localized reduction in proteoglycan content can be detected with CECT. The current resolution in the CT imaging of extremities with an ethically acceptable radiation dose is 200-700 µm [14,15].

Although magnetic resonance imaging (MRI) is expensive and has limited availability, it is becoming more routine in the diagnostics of OA and cartilage injuries. MRI has high soft tissue contrast and it can be used to detect cartilage lesions. MRI techniques have also been developed for quantitative analysis of cartilage degeneration [57–59]. There are novel techniques that could aid in diagnostics of early OA, *e.g.* T2 relaxation mapping which is sensitive both the water content and the organization of collagen fibril network [60–62] and delayed gadolinium-enhanced MRI that reveals the changes in proteoglycan content [59,63]. However, the limited resolution of MRI imaging (in plane resolution 300-600 µm [16]) means that it has rather low sensitivity at detecting small and early stage degeneration [64].

Conventional arthroscopy is a minimally invasive technique, which is usually conducted for diagnostics or while conducting a surgical operation like meniscus or ligament repair. During arthroscopy, the condition of cartilage, menisci, and ligaments can be assessed. Articular surface can be visualized with a camera, whereas cartilage softening may be estimated by palpation. This technique is good for the detection of softening or fibrillation of cartilage surface, substantial cartilage loss, and injuries. The severity of cartilage injuries can be graded using the International Cartilage Repair Society (ICRS) scoring system [65]. In this system, the lesion depth relative to the cartilage thickness is evaluated (Table 2.1). However, as arthroscopy achieves only a visualization of the cartilage surface, neither the lesion depth nor the cartilage thickness can be measured accurately. Furthermore, subsurface lesions are not visible at all. Due to the subjective nature of arthroscopic lesion scoring, its intra- and inter-observer reproducibility have been found to be poor [18–20].

Arthroscopic ultrasound imaging has been proposed as an approach to support conventional arthroscopy [66, 67]. Cartilage lesions can be detected, thickness estimated and the roughness of the cartilage surface measured from the ultrasound image [68, 69]. Ultrasound reflection and backscattering are known to reflect the biomechanical and compositional properties of articular cartilage and subchondral bone [70, 71]. Moreover, the speed of ultrasound in cartilage has been found to decrease in conjunction with the development of tissue degeneration [72, 73]. Thus, ultrasound could be used for quantitative assessment of cartilage. Another potential technique complementary to conventional arthroscopy is optical coherence tomography, a technique which is the focus of this doctoral thesis.

Table 2.1: ICRS scoring criteria for severity of cartilage injury [65].

Score	**Criteria**
ICRS 0	Cartilage is macroscopically normal, no notable defects
ICRS 1	Fibrillation and/or slight softening of the surface, possibly superficial lacerations and fissures
ICRS 2	Defect deeper than in class ICRS 1, but <50% of cartilage thickness
ICRS 3	Defect having depth of >50% of cartilage thickness, but not extending through subchondral bone
ICRS 4	Defect extending into the subchondral bone

3 Optical coherence tomography

Optical coherence tomography (OCT) is an imaging technique which provides high resolution cross-sectional images of soft tissues to a depth of about 2 mm [74]. The contrast in the OCT image is based on differences in light backscattering properties of tissue structures. A light beam is directed to the sample and part of it scatters back to the detector from the small scatterers within the depth of the sample. By using a low coherence interferometer, the intensity of the backscattered light is measured as a function of depth. The intensity measurement is repeated in adjacent locations in order to obtain a two- or three-dimensional image [74].

OCT has been most commonly applied in ophthalmology. OCT is able to image the structures of an eye with a resolution of about 10 µm, *i.e.* a better resolution than achieved by any other non-invasive ophthalmic imaging technique. It is a clinical standard in the diagnosis of many retinal diseases and its use in the diagnosis and monitoring of macular diseases, glaucoma and diabetic retinopathy is increasing [75,76]. Quantitative analysis is possible, such as in the measurement of the retinal nerve fiber layer thickness [77]. Another wide-spread clinical use for OCT is intravascular imaging. OCT is used to measure lumen size, to recognize lesions within the artery wall, and to assess stenosis [78,79].

Additionally, OCT has been used for studying structural features or identifying pathological changes for example in skin [80] and gastrointestinal tract [81]. The OCT technique has also been adopted in engineering applications, such as in the measurement of paper or coating properties [82,83]. OCT is applicable as long as there is sufficient light penetration.

3.1 TIME DOMAIN OCT

The traditional OCT system is based on low coherence interferometry. Usually, a Michelson interferometer, where the sample arm mirror is replaced with a sample, is employed to resolve the backscattering within the sample as a function of depth [74]. A schematic diagram of an interferometer used in OCT systems is presented in Figure 3.1. The input light wave from the source is divided by a beam splitter into two components. The first beam is directed to the reference arm and the other to the sample arm. The waves are reflected from the reference mirror and a reflector in the sample, and subsequently recombined by the beam splitter.

The light intensities returning from the reference and sample arms are the time averages of the square of the corresponding electric fields E_r and E_s [84]:

$$I_r = \langle [E_r(t+\tau)E_r^*(t+\tau)] \rangle \tag{3.1}$$

$$I_s = \langle [E_s(t)E_s^*(t)] \rangle \,. \tag{3.2}$$

The intensity at the detector can be described as

$$I_D(\tau) = \langle [E_s(t) + E_r(t+\tau)][E_s(t) + E_r(t+\tau)]^* \rangle \,, \tag{3.3}$$

where $\tau = \Delta L/c$ is the time delay between the two beams caused by optical path length difference ΔL between the reference and sample arms. c is the speed of light. By applying the equations (3.1) and (3.2), $I_D(\tau)$ can be rewritten as [84,85]

$$I_D(\tau) = I_r + I_s + 2\sqrt{I_r I_s}|\gamma_{sr}(\tau)| \cos(2\pi f_0 \tau) \,, \tag{3.4}$$

where γ_{sr} is the degree of the coherence of two interfering electric fields. The cosine term is caused by the phase difference occuring due to the different optical paths in the two arms and f_0 is the center frequency of the source. When the reference mirror is moved with a constant velocity, a Doppler shift f_D occurs and I_D becomes

$$I_D(\tau) = I_r + I_s + 2\sqrt{I_r I_s}|\gamma_{sr}(\tau)| \cos(2\pi f_D t) \,. \tag{3.5}$$

The latter part of the equation is the signal carrying part that depends on the coherence of the interfering electric fields. $\gamma_{sr}(\tau)$ varies between 0 and 1 depending on the path length mismatch according to the equation

$$|\gamma_{rs}| = \mathrm{e}^{-4(\Delta L/L_c)^2}, \tag{3.6}$$

where L_c is the coherence length describing the length over which the two interfering fields are coherent [84]. In fact, γ_{sr} is the Fourier transform of the power spectral density of the light source and it depends on the shape, bandwidth and the central wavelength of the source field [86].

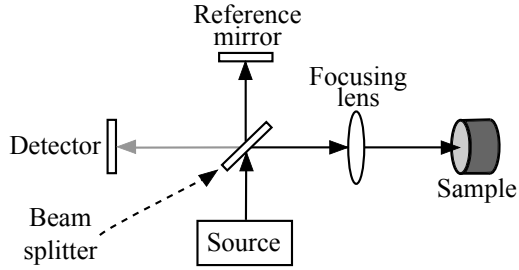

Figure 3.1: Schematic diagram of an interferometer within an OCT system. Broadband light coming from the source is divided into sample and reference arms (black arrows). The light reflects back from the reference mirror and the sample, and is recombined by the beam splitter. The recombined wave (grey arrow) is detected with the detector.

3.2 FOURIER DOMAIN OCT

Fourier domain OCT imaging (FD-OCT) can be conducted using two techniques; spectral domain (SD-OCT) and swept source OCT (SS-OCT) techniques. In SD-OCT systems, a broadband light source is used and the mirror in the reference arm of the interferometer is fixed in position, an approach which enables faster data acquisition. Interference of the reference arm electric field and the field reflected from a single reflector in the sample form a periodic fringe in the k-space. A larger optical path length difference between the two

arms causes the fringe to have a higher frequency. In practice, there are multiple scatterers within the depth of the sample and the superimposed spectrum enters the spectrometer used as the detector. The depth information can be obtained from the inverse Fourier transform of the spectrum backscattered from the sample [87, 88]. The spectral interference signal is measured with a detector array, *e.g.* a CCD detector. The equation (3.4) applies also in SD-OCT, but in this case, it is frequency dependent [85].

SS-OCT uses a tunable light source instead of a broadband source [87]. A narrow bandwidth is rapidly tuned through a broad bandwidth and a single photodetector can be used to measure the interference signal sequentially as a function of time [85]. FD-OCT has higher sensitivity and it is a much faster technique than the time domain OCT [89, 90].

3.3 RESOLUTION

When the light source has a Gaussian frequency spectrum, which is usually the case, the coherence length, *i.e.* the full-width-at-half-maximum (FWHM) of the field autocorrelation function in air, is [85]

$$L_c = \frac{2\ln 2}{\pi}\frac{\lambda_0^2}{\Delta\lambda}, \tag{3.7}$$

where λ_0 is the central wavelength of the source and $\Delta\lambda$ is the wavelength range, (*i.e.* the FWHM of the source power spectrum). In a medium other than air, the coherence length is $L_{c,medium} = L_c/n_{medium}$, where n_{medium} is the group refractive index of the medium. The resolution of OCT in the light propagation direction, *i.e.* the axial resolution, equals the coherence length [74, 85]. Thus, the resolution is inversely related to the spectral bandwidth of the source. However, the bandwidth cannot be increased excessively since the dispersion will start to affect the image. Current OCT systems can achieve resolutions of 1-15 µm [91].

Lateral resolution (δx) of OCT depends on the lateral scanning frequency and the beam diameter. At its best, it is the FWHM

of intensity of the beam at the narrowest point of the beam, the waist [92]:

$$\delta x = 0.37 \frac{\lambda_0}{NA}, \tag{3.8}$$

where NA is the numerical aperture of the system.

3.4 LIGHT AND TISSUE

When light is directed onto tissue, it encounters particles such as atoms and molecules. Depending on the energy of the incident photon, the particles can either absorb or scatter light. There is a certain energy that an electron of an atom requires for transition to a higher energy state. If the energy of the photon equals this energy, then the light will be absorbed and the atom becomes excited. If the energy is not sufficient to excite the atom, the electrons of the atom start to oscillate with respect to positively charged nucleus and an oscillating dipole is created. This oscillating dipole creates a secondary electromagnetic field which is the scattered light [93,94].

Absorption and scattering cause light attenuation in tissue. OCT light sources usually have central wavelengths around 800 nm or 1300 nm. In soft tissues, absorption of these wavelengths is low compared to scattering. Thus, the light attenuation is mainly due to scattering [93]. A wavelength of around 800 nm is used in ophthalmic imaging to obtain high resolution, whereas highly scattering media usually require longer wavelengths in order to achieve better light penetration. However, water absorption becomes significant at 1380-1600 nm and 1900-2000 nm wavelengths, and thus these wavelengths should be avoided since they give rise to excessive light attenuation [91].

An OCT system works on the assumption that the received light is scattered only once [95]. Light scattering within a tissue is determined by the scatterer size, shape and density relative to the wavelength and the refractive index between the medium and the scatterers [93]. In tissues, the particles scattering the light (*e.g.* cells

and macromolecules) are mostly larger than the wavelengths used in OCT sources [93].

A single particle that is small compared to the wavelength scatters light equally in all directions. In tissues, scattering particles like cells are constructed from several oscillating molecules. Different molecules of the particle separately interact with the light and the fields scattered from them interfere either constructively or destructively. In forward scattering, the constructive interference will predominate whereas in other directions, more destructive interference occurs. Thus, the forward scattering becomes the strongest and this, together with attenuation, limits the depth field of view of OCT because OCT measures backward scattered light [93, 94]. When imaging living tissues, the intensity of the source light must be limited in order to avoid excessive heating due to absorption. In soft tissues, the OCT imaging depth is limited to about 2 mm.

The intensity of backscattered light measured with OCT depends on the structure and composition of the tissue. The size of the scatterers relative to the wavelength affect the angle dependence of the scattering whereas the probability of scattering depends on the density, size and refractive index of the scatterers. Thus, structural and compositional changes in the tissue could possibly be detected as changes in OCT-measured backscattering.

3.5 OPTICAL COHERENCE TOMOGRAPHY OF ARTICULAR CARTILAGE

OCT has been evaluated as a promising tool for the detection of cartilage injuries and degeneration. Current technology enables the manufacturing of small OCT probes that can be used during arthroscopic examination. Arthroscopic OCT has been conducted not only in animal joints [22, 26, 96] but also in human knee and carpometacarpal joints [21, 97–100]. Arthroscopic OCT could be valuable in diagnostics because the degree of cartilage damage may be underestimated if it is assessed only with conventional arthroscopy [21].

As OCT provides cross-sectional images instead of only a surface image, it has very good resolution. It allows quantification of surface roughness as well as a detection of surface fibrillation that matches with histological findings [21, 25, 101–104]. Cartilage that seems intact in conventional arthroscopy may exhibit small superficial or subsurface lesions that can be detected with OCT [21, 22]. The determination of lesion type and severity is more accurate when conducted based on an OCT image, because this enables the measurement of both the extent and the depth of the lesion [22, 96]. Furthermore, cartilage thinning, which is impossible to measure using conventional arthroscopy, can be detected with OCT [101, 102]. OCT could also have a role in the detection of osteoarthritic changes at the cartilage-bone interface [101, 105, 106].

A more quantitative approach is needed when cartilage degeneration needs to be diagnosed before any visual sign of rupture or fibrillation can be seen. Early stage changes in collagen fibril orientation or chondrocyte and proteoglycan content may alter the birefringence or the light scattering properties of the tissue and, therefore, affect the OCT image. By using OCT-measured light backscattering, Bear *et al.* (2010) examined the effect of an injury with an impact energy sufficiently low not to create any visible damage but high enough to cause cell death [107]. These investigators found that the impact changed the relationship between the light backscattering levels at certain depths, which could be related to the extent of degeneration of the collagen matrix.

Polarisation sensitive OCT (PS-OCT) provides more information on the orientation of collagen fibrils. Articular cartilage is birefringent because of its highly organized collagen network [108]. The collagen alignment in healthy cartilage changes approximately from being horizontal in the cartilage surface to vertical in the deep zone. Thus, the light scattered from different depths within cartilage has varying polarization states that can be visualized with PS-OCT [23]. PS-OCT can be conducted by using either a single or dual detector technique. In the single detector technique, birefringent articular cartilage causes banding patterns within the image.

When the light originating from the sample and reference arms have similar polarization states, a bright band occurs, whereas orthogonal polarization states evoke a dark band. When the collagen network becomes disrupted and disorganized, the birefringence is reduced and the banding pattern becomes diminished, even completely lost [102, 105]. With the dual detector technique, the light of two orthogonal polarization states is detected separately and a phase retardation image is constructed [109]. The retardance profile enables quantification of birefringence [110]. Furthermore, the polarization properties of tissue can be studied by determining its Jones matrix [111].

OCT could be valuable in the estimation of cartilage healing after injury or repair surgery. Han *et al.* (2003) evaluated the use of OCT in the structural evaluation of cartilage repair, conducted by implanting allogenic cultured chondrocytes embedded in collagen gels into the defect and covering the gels with autologous periosteum [112]. It was noted that OCT was able to monitor the integration of repair tissue with the surrounding healthy cartilage and it could detect repair tissue hypertrophy and structural inhomogeneity. In the study of Virén *et al.* (2012), spontaneously repaired tissue with a lower collagen network organization and smaller collagen and proteoglycan contents than adjacent intact cartilage, showed lower surface reflections and more backscattering than intact cartilage [104]. Furthermore, spontaneously repaired tissue was found to display a significantly lower light attenuation coefficient than healthy cartilage [25].

4 Aims of the thesis

This doctoral thesis assessed the use of optical coherence tomography in the evaluation of articular cartilage.

The specific aims of this thesis were:

- To investigate whether the compositional or structural changes in articular cartilage could be detected through the measurement of light backscattering and attenuation using optical coherence tomography.
- To develop an arthroscopic technique utilizing simultaneous ultrasound imaging and optical coherence tomography for the measurement of speed of sound in articular cartilage.
- To study the feasibility of optical coherence tomography in the arthroscopic evaluation of articular cartilage and in the assessment of the success of surgical articular cartilage repair.

5 Materials and Methods

The thesis consists of studies **I-III** as well as of unpublished data (studies **A** and **B**). The materials and methods utilized in the studies are summarized in this section (Figure 5.1).

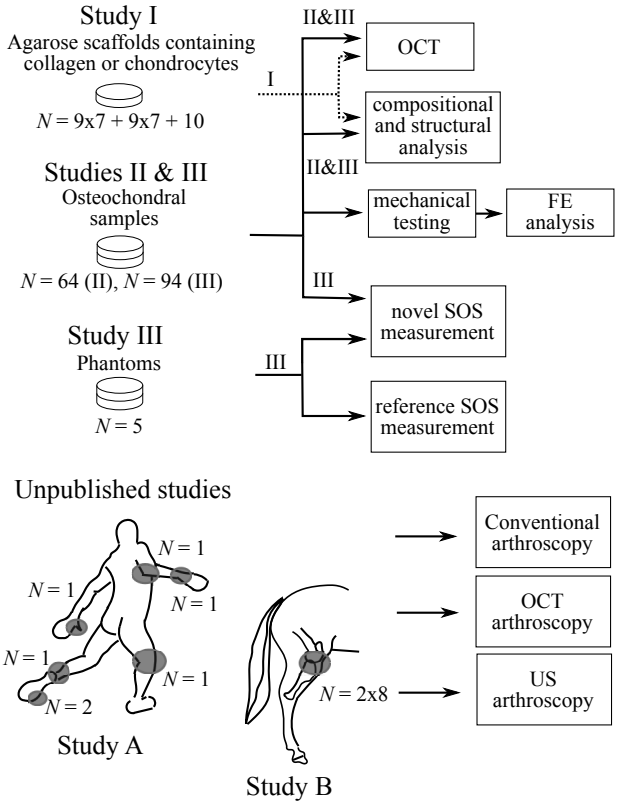

Figure 5.1: Summary of the materials and methods applied in the studies. FE analysis = finite element analysis, US = ultrasound, SOS = speed of sound.

5.1 MATERIALS

5.1.1 Agarose scaffolds

In study **I**, varying amounts of collagen and chondrocytes were embedded into 4% agarose gel scaffolds. Chondrocytes were extracted from cartilage of bovine femoral condyles obtained from a local abattoir (Atria Oyj, Kuopio, Finland). The chondrocytes were counted and the desired quantity was mixed into an agarose gel. Type I collagen (Sigma-Aldrich, St Louis, MO, US), in turn, was dissolved into hydrochloric acid and the desired amount of this suspension was diluted in agarose gel. The gel suspensions were subsequently pipetted into wells having a height of 3.9 mm and a diameter of 5.9 mm to form a cylindrical gel sample. The surface of the sample was flattened with a glass plate.

A total of nine chondrocyte sets, each including seven agarose scaffolds with different chondrocyte densities (0, 1, 2, 4, 8, 16, and 32 million cells/ml) and nine sets of gel scaffolds with varying collagen concentration (0, 1.5625, 3.125, 6.25, 12.5, 25, and 50 mg/ml) were prepared. The collagen concentration in normal articular cartilage is close to 200 mg/ml. Although scaffolds with higher collagen concentration were at first found difficult to prepare, an additional collagen set including nine agarose scaffolds with a collagen concentration of 100 mg/ml and a control scaffold without any collagen was successfully made.

5.1.2 Phantoms

In study **III**, five phantoms were used to investigate the accuracy of the SOS measurement technique based on simultaneous ultrasound and OCT imaging. SOS in the phantom materials obtained with this technique were compared to those measured with a reference technique based on a custom-made acoustic microscope (central frequency 50 MHz, -6 dB bandwidth 30-73 MHz, focal length 25 mm, sampling frequency 550 MHz) and a caliper (resolution 10 µm; DIGI-MET 1226 417, Helios-Preisser, Germany). Phantom ma-

terials were 2% and 4% agarose hydrogels, silicone rubber, glass, and acrylonitrile butadiene styrene. The thickness of these phantoms was between 0.5 mm and 2.2 mm. Their refractive indices were determined using the modified optical path length shifting method [113].

5.1.3 Equine osteochondral samples

Eighteen metacarpophalangeal joints of skeletally mature horses were obtained from a slaughterhouse. A total of 94 osteochondral blocks were prepared mainly from the medial and lateral sides of the proximal phalanx (P1; N = 34), dorsoproximal areas of the condyles of the third metacarpal bone (MC3; N = 34), and from the sagittal ridge (SR; N = 21) of the third metacarpal bone. Additionally, five blocks were prepared from other locations, where injuries were encountered. Osteochondral blocks had a minimum surface area of 1×1 cm^2. The blocks were cut so that the possible lesion was placed in the middle and the site of interest was marked with a felt-tip pen. All 94 samples were included in study **III**, whereas 64 samples with the clearest tidemark in the OCT images were included in study **II**.

5.1.4 Human cadavers

In the human cadaver studies (study **A**), an elbow, first metatarsophalangeal (MTP1) and metacarpophalangeal (MCP1) joints and a wrist of a female cadaver (age 86 years) and an ankle, a knee, and an MTP1 of another female cadaver (age 95 years) underwent conventional, OCT, and ultrasound arthroscopies. Cadavers were obtained from Kuopio University Hospital after receiving ethical approvals from the ethical committee of Kuopio University Hospital (permission number 18/2012) and from the National Supervisory Authority for Welfare and Health (Valvira; 1410/06.01.03.01/2012). The arthroscopies were conducted by experienced orthopaedic surgeons.

5.1.5 Shetland ponies

In study **B**, eight Shetland ponies of age 7 ± 4 years (mean $\pm$ SD) and weight 191 ± 28 kg underwent an open joint surgery, where two cylindrical ostechondral defects (diameter 10 mm) were created on both of their stifle joints. The four defects were repaired with four different techniques. First, ten microfractures were created in the subchondral bone of all the defects. In repair technique 1, the defect was filled with fibrin glue [114] which contained 2 million cells/ml (20% chondrons and 80% mesenchymal stromal cells). In repair technique 2, a gelatin methacrylamide (GelMA; [115, 116]) hydrogel with embedded cells (20 million cells/ml) was used to fill the defect. The GelMA was then crosslinked with ultraviolet light. In repair technique 3, one million cells were infused into the bottom of the defect with a small amount of GelMA. The defect was then filled with cell free GelMA, which was crosslinked with ultraviolet light. In repair technique 4, three scaffolds prepared from 14-µm-thick polycarpolactone (PCL) fibers stacked in a mesh (thickness 0.5 mm, porosity 92%) were placed on top of each other in the defect to increase the stiffness of GelMA/cell suspension which was used to subsequently fill the defect [117]. The cell content of the suspension was 20 million cells/ml. Again, the GelMA was crosslinked with ultraviolet light.

The surgical procedures were conducted in the Department of Equine Sciences of Utrecht University by experienced surgeons. The study was approved by the Utrecht University Ethics Committee for Animal Experiments. Study **B** is part of a one-year follow-up study where different articular cartilage repair techniques are tested and the healing of cartilage are being followed at four time points; 0, 2, 6 and 12 months after the repair.

5.2 OCT IMAGING

OCT SYSTEM

A commercial OCT system (Ilumien PCI Optimization System, St.

Jude Medical, St Paul, MN, USA), originally designed for intravascular imaging, was used in all of the studies. This system was chosen based on the size and flexibility of its imaging probe (C7 Dragonfly, St. Jude Medical), which could enable its arthroscopic use. The system has a light source with central wavelength of 1305 nm and $\pm$55 nm wavelength range. Light is directed into a rotating optical fiber (100 rotations/s). At the tip of the fiber, light is directed to leave the fiber at an approximately perpendicular angle. During each rotation, the system records 504 axial scan lines to provide a cross-sectional image of the surrounding tissue (Figure 5.2). With an automatic pullback system, 541 adjacent cross-sections (thickness 0.1 mm) along the probe axis direction can be recorded within seconds. The optical fiber is shielded by a flexible cover tube which has a diameter of 0.9 mm. According to the manufacturer, the axial and lateral resolutions of the system are $\leq$20 µm and 25-60 µm, respectively.

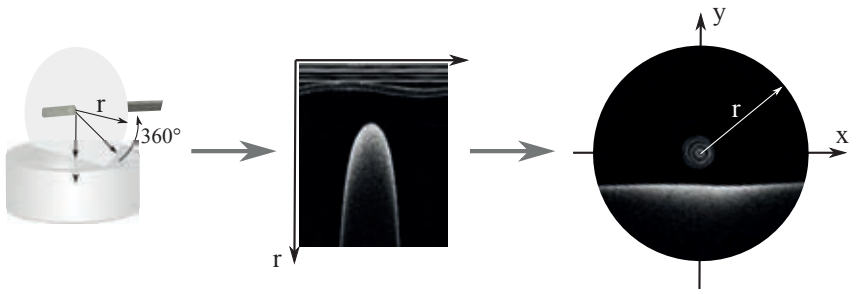

Figure 5.2: The imaging probe of the OCT system rotates and produces a cross-sectional image during each rotation. The raw image in polar coordinates is processed into an image in Cartesian coordinates.

Human cadaver arthroscopies

First, the feasibility of using the OCT system in arthroscopic examination was studied by conducting conventional, OCT, and ultrasound arthroscopies on multiple human cadaver joints (study **A**). Joint space was pressurized with physiological saline and normal arthroscopic portals were created. Intact and degenerated cartilage

sites were first identified using conventional arthroscopy. The same areas were then imaged with OCT using the automatic pullback-system and with ultrasound. OCT was also used to detect additional lesions that were not seen during the arthroscopic examination. The OCT and ultrasound probes were inserted into the joint through a separate custom-made instrument channel, or the instrument channel of the arthroscope (Figure 5.3). The probes were guided under arthroscopic view in all joints except in the MCP1. Applicability and feasibility of OCT arthroscopy were qualitatively evaluated and compared with those of conventional and ultrasound arthroscopy.

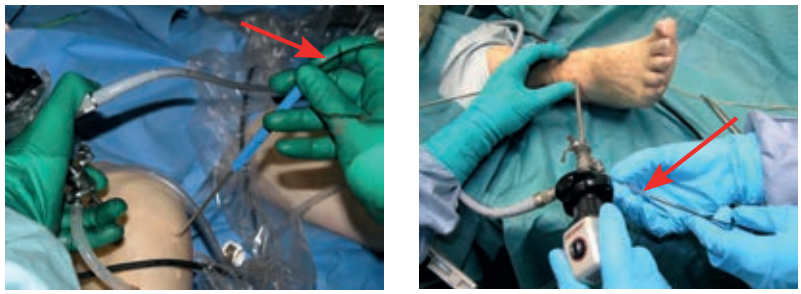

(a) *(b)*

Figure 5.3: OCT arthroscopy setup. The thin OCT probe (red arrow) was inserted into the joint through an instrument channel, which was either (a) separate from or (b) integrated into the arthroscope.

In one knee, ankle, and MTP1 joint, OCT imaging was conducted simultaneously with ultrasound imaging. The intravascular ultrasound system (Clear View Ultra, Boston Scientific Corporation, San Jose, CA, USA) used for this was equipped with an almost identically sized probe as the OCT system (diameter 1 mm; Atlantis TM SR Pro, Boston Scientific Corporation) using a rotating ultrasound transducer (30 rounds/s, 255 A-scan lines per rotation, center frequency 40 MHz, -6 dB bandwidth 30.1-45.3 MHz, pulse length 0.124 µs). The probes were simultaneously inserted into the joint through

the instrument channel of an arthroscope. The OCT images and ultrasound videos obtained simultaneously from the same site were recorded and compared qualitatively.

Imaging of the agarose gel samples

In study **I**, the agarose gel samples and the OCT probe were embedded in phosphate-buffered saline (PBS). The probe was aligned parallel to the sample surface with the help of a goniometer (Edmund Industrial Optics, York, UK). Each sample was scanned with OCT four times. The scanning was conducted throughout the width of the sample and the probe was realigned between each repetition.

Imaging of the osteochondral samples

The osteochondral blocks in studies **II** and **III** were also imaged in a bath containing PBS. To mimic arthroscopic conditions in alignment of the probe, the probe was hand-held above the site of interest during the OCT scanning. The site of interest within each block was scanned once using the automatic pullback system.

Imaging of the repaired joint surfaces

In study **B**, the repaired cartilage defects and the surrounding healthy cartilage in the joints of the ponies were imaged with OCT. Immediately after the repair, the defect site and the surrounding cartilage were imaged with OCT and ultrasound. Scan lines covering the central part of the defect, the surrounding cartilage and the interface between the repair tissue and surrounding cartilage were predefined (Figure 5.4). A thin layer of physiological saline was maintained on the cartilage surface to ensure that the imaging probes were immersed in saline.

The success of the repair was evaluated two months after the repair surgery by conducting conventional, OCT and ultrasound arthroscopy. Similarly as in human cadaver arthroscopies, the joint

space was pressurized with physiological saline. The same scan lines as in the first time point were used in the OCT and ultrasound arthroscopies.

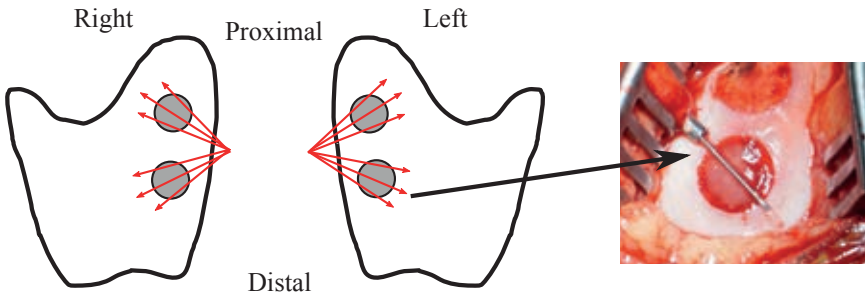

Figure 5.4: Predefined scanlines (red arrows) for OCT and ultrasound imaging of the repaired defects in right and left stifles of ponies. Diameter of the defects was 10 mm.

5.3 SPEED OF SOUND MEASUREMENTS UTILIZING OCT AND ULTRASOUND IMAGING

Measurement technique

A novel method for arthroscopic measurement of SOS in cartilage was developed in the present thesis. This technique combines simultaneous measurements of cartilage thickness with OCT and the travel time of high frequency ultrasound pulse, *i.e.* time-of-flight (TOF) in cartilage with the same ultrasound imaging system as used in studies **A** and **B**. An oval instrument channel was designed to the keep the imaging heads of the probes adjacent to each other during the measurement and to enable the insertion of the catheters through a normal arthroscopic portal (Figure 5.5). The largest outer diameter of the instrument was 3.33 mm. Ultrasound A-scan lines constructing the ultrasound image were recorded with sampling frequency of 250 MHz, while the same site was scanned with OCT.

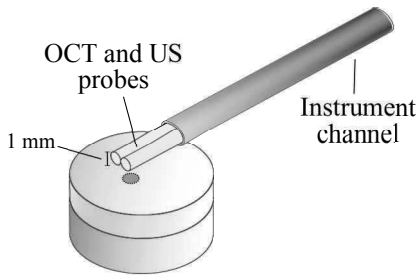

Figure 5.5: Setup of the technique combining simultaneous OCT and ultrasound imaging for the arthroscopic measurement of SOS. OCT and ultrasound (US) probes are positioned with a custom-made instrument channel so that the imaging heads of the probes were kept adjacent to each other. The measurement area is a small, approximately 1×1 *mm*^{2} *area under the ultrasound probe.*

Measurement of SOS in phantoms

SOS in phantoms and cartilage were measured with the developed technique (study **III**). The sample and the probes were immersed in degassed distilled water during the measurements. The sample was aligned with a goniometer to direct the ultrasound beam perpendicular to the sample surface. For the phantoms, SOS was measured five times without repositioning the probe between the measurements. Each of the five measurement included a recording of ten subsequent cross-sectional ultrasound images and simultaneous recording of 10 adjacent cross-sectional OCT images from the same location. This imaging set of five measurements was repeated three times to evaluate the reproducibility of the measurements. The instrument was repositioned between the three repetitions.

Measurement of SOS in equine cartilage *in vitro*

The SOS in cartilage was measured five times for each sample. The sample and the probes were immersed in degassed PBS during the imaging. Instrument alignment was done manually in order to mimic the arthroscopic conditions.

Arthroscopic measurement of SOS in human cartilage

The arthroscopic use of the technique for SOS measurement was tested in a human cadaver ankle. The joint was pressurized with physiological saline. The OCT and ultrasound probes were inserted into the joint through the instrument channel of the arthroscope and SOS of articular cartilage was measured in twelve locations. In three locations, the measurement was repeated twice and the average SOS was determined. In other locations only one measurement per site was conducted.

5.4 REFERENCE TECHNIQUES

5.4.1 Biomechanical measurements

Biomechanical measurements were conducted *in vitro* for the equine samples examined in studies **II** and **III**. A stress-relaxation testing was performed using a custom-made material testing system equipped with a plane-ended indenter (diameter 530 µm). Prior to the indentation testing, cartilage thickness at the measurement site was determined with OCT. The stress-relaxation test included two indentation steps (both 5% of cartilage thickness). The strain rate was 100%/s relative to the cartilage thickness and after indentation, cartilage was allowed to relax until the slope of relaxation was less than 10 Pa/min.

The mechanical properties of cartilage were determined through fitting an axisymmetric fibril-reinforced poroelastic finite element model of cartilage to the experimental data [118–123]. Proteoglycans and the porous structure filled with fluid were modelled with a biphasic porohyperelastic non-fibrillar matrix and collagen network with elastic fibrillar matrix. A fibril network modulus (E_f) expressing the collagen matrix behaviour under indentation, a non-fibrillar matrix modulus (E_m) expressing the behaviour of the non-fibrillar matrix, and the permeability (k) of the modelled material

were determined through optimization of the model to the second indentation step.

5.4.2 Compositional and structural analysis

Agarose scaffolds (study **I**) and osteochondral samples (studies **II** and **III**) were prepared for compositional and structural analyses. The sample preparation for histological examination followed the standard protocols including formalin fixation, decalcification of the osteochondral blocks with ethylenediaminetetraacetic acid (EDTA), paraffin wax embedding, and cutting into sections [124].

Light microscopy and digital densitometry

Three histological sections (thickness 3 µm) were obtained from the site of interest in the osteochondral samples (studies **II** and **III**). The sections were stained with a cationic dye (Safranin-O), which binds stoichiometrically to negatively charged glycosaminoglycan groups. The stained sections were then imaged with a light microscope (Axio Imager M2, Carl Zeiss MicroImaging, Jena, Germany) and a digital densitometer consisting of a light microscope (Leitz Orthoplan, Leitz, Wezlar, Germany) and a CCD camera (SenSys, Photometrics Inc., Huntington Beach, CA, USA). To evaluate the integrity of cartilage, the microscopic images were graded by three investigators using the Mankin score [125]. The scores awarded by the investigators for the three sections were averaged and the average score was rounded to the nearest integer. In study **II**, the samples were also divided into two groups according their Mankin score; from no to mild degeneration (Mankin score 0-6) and from moderate to severe degeneration (Mankin score 7-14) [126]. Optical density (OD), which is related to tissue fixed-charge density, *i.e.* the proteoglycan content [124, 127] of the samples was determined by means of digital densitometry. The depth-wise OD curve and the average OD within each section were determined.

In study **I**, histological sections (thickness 10 µm) from agarose scaffolds with chondrocytes were stained with hematoxylin and

eosin. Sections (thickness 5 µm) from the scaffolds with collagen were stained with Masson's trichrome. Representative sections from each scaffold type were imaged with the light microscope and the distribution and relative content of chondrocytes or collagen was evaluated.

Fourier transform infrared spectroscopy

Light absorbance of different chemical bonds depends on the wavelength of the light. This property can be used to determine the chemical composition of a sample. Fourier transform infrared spectroscope (FTIR; Spotlight 300 FTIRI, Perkin Elmer, Shelton, CT, USA) was used to measure the light absorbance in specific spectral areas in order to evaluate the collagen (studies **II** and **III**) and proteoglycan (study **III**) distributions in three unstained sections (thickness 5 µm) prepared from the osteochondral samples. Absorbance was calculated by measuring the areas under the absorption spectra at 1585-1720 cm^{-1} (amide I region) and 984-1140 cm^{-1} (carbohydrate region) for obtaining the distribution of collagen and proteoglycans, respectively [128,129]. The absorbance in the region 1600-1700 cm^{-1} was measured in order to assess the relative collagen contents in one agarose scaffold of each type in study **I** [130].

Polarized light microscopy

Collagen network organization of the osteochondral samples in studies **II** and **III** were investigated with polarized light microscopy. In this technique, light is polarized with a linear polarizer and a second polarizer is rotated with respect to the first polarizer so that no light passes through the pair. When a birefringent sample is placed between the pair of polarizers, the polarization state of the light changes so that some light passes through the system. The polarizer pair is rotated stepwise and the image at each step is recorded. A polarized light microscope (Ortholux II POL; Leitz Wezlar, Wezlar, Germany) equipped with a CCD camera (Photometrics) was

used to determine the collagen orientation and its anisotropy (parallelism index, PI) in three unstained sections (5 µm) prepared from the osteochondral samples. Collagen fibril organization was determined by calculating the Stokes parameters [131]:

$$\begin{aligned} S_0 &= I_{(0^\circ)} + I_{(90^\circ)}\,, \\ S_1 &= I_{(0^\circ)} - I_{(90^\circ)}\,, \\ S_2 &= 2 \cdot I_{(45^\circ)} - S_0\,, \\ S_3 &= S_0 - I_{(90^\circ + \lambda/4)}\,. \end{aligned} \tag{5.1}$$

$I_{(0^\circ)}$, $I_{(45^\circ)}$, $I_{(90^\circ)}$ and $I_{(90^\circ+\lambda/4)}$ are the measured light intensities in background-corrected 0°, 45°, 90° images and 90° image taken with a $\lambda/4$ phase shifter, respectively. S_0 is the total light intensity, S_1 is the intensity of the light with linear horizontal or vertical polarization, S_2 is the intensity of the light with linear $+45^\circ$ or -45° polarization and S_3 is that of the light with circular polarization. The orientation angle of polarization ellipse is then [131]:

$$\Psi = \frac{\arctan(\frac{S_2}{S_1})}{2}, \quad 0^\circ \leq \Psi \leq 90^\circ\,. \tag{5.2}$$

Ψ is directly related to the orientation of the collagen network [132].

PI is determined by measuring the minimum and maximum intensities (I_{min} and I_{max}, respectively) of the light at different polarizer settings [132]:

$$\mathrm{PI} = \frac{I_{max} - I_{min}}{I_{max} + I_{min}}\,. \tag{5.3}$$

PI varies between 0 and 1, *i.e.* from completely random fibril orientation to completely organized orientation where the fibrils lie parallel to each other.

5.5 DATA ANALYSIS

5.5.1 Arthroscopic data

The applicability and feasibility of arthroscopic OCT were evaluated qualitatively in the two unpublished studies **A** and **B**. Study

A compared the ease of identification of the structural features of cartilage in small and large human joints with conventional arthroscopy, OCT and ultrasound. The strengths and weaknesses of these techniques were assessed. In study **B**, the use of OCT in analyzing the success of cartilage repair was investigated with surgically repaired equine cartilage *in vivo*. The abilities of conventional arthroscopy, OCT, and ultrasound to detect and identify the structure of repair tissue were evaluated. Furthermore, the integration of the repair tissue to the surrounding cartilage and the integrity of the surrounding cartilage were determined.

5.5.2 Attenuation and backscattering coefficients

Total attenuation and backscattering coefficients (μ_t and μ_b, respectively) in studies **I** and **II** were determined from the depth-dependent OCT signals ($b\,(d)$) measured from the samples. Light attenuation in the tissue follows Beer-Lambert law, and therefore the light intensity decays exponentially as a function of penetration depth. The total attenuation coefficient describes the rate of the attenuation. Assuming that OCT detects only once scattered photons, the dependence of $b(d)$ on μ_t and μ_b can be described as follows [133]:

$$b(d) \propto \sqrt{\mu_b} \exp\left(-\mu_t d\right) , \tag{5.4}$$

where d is the probing depth, *i.e.* the depth where the backscattered signal is measured. Due to the focusing, the intensity profile of the light beam in the propagation direction is Gaussian. Therefore, the amount of light backscattering measured from different depths depends not only on the attenuation, but also on the distance between the focus position (d_0) and the probing depth. Thus, the OCT signal affected by the focusing can be described as [134]:

$$b(d) \propto \frac{\sqrt{\mu_b}}{\sqrt{\left(\frac{(d-d_0)}{z_0}\right)^2 + 1}} \exp\left(-\mu_t d\right) , \tag{5.5}$$

where z_0 is the apparent Rayleigh length of the light beam describing the depth of focus. The OCT system was calibrated using a suspension series of water and varying concentrations of polystyrene spheres ($n_{\text{polystyrene}}$ = 1.57, diameter 5 µm; Phosphores Inc., Hopkinton, MA, USA) with known μ_t and μ_b [135]. The mass of the polystyrene spheres relative to the mass of the water in these suspensions were 0.33%, 0.20%, 0.14%, 0.11%, 0.09%, and 0.08%. The depth-dependent OCT signals obtained from the six suspensions were then fitted into equation 5.5 with the assistance of a system specific calibration constant. This constant was resolved separately from the six measurements and the average calibration constant was used to calculate the total attenuation and backscattering coefficients of the samples in studies **I** and **III**.

μ_t and μ_b of the agarose scaffolds

In study **I**, the depth-dependent OCT signal of each sample was calculated from the raw OCT image in polar coordinates. The scaffold surface was detected semi-automatically; two windows were manually placed on the image, the first on the background area and the second on the area of the scaffold surface. The scaffold surface was then automatically detected from the latter window using a threshold value determined from the first window. The threshold value was set to +3 SD of the mean grayscale value within the background window. In the OCT image in polar coordinates, the surface point closest to the catheter is the one to which the incident light beam is perpendicular. This point was found by first filtering the detected surface profile with a three-point moving average filter and then by searching for the maximum of a fourth degree polynomial function fitted to it. An average intensity profile was determined for a region of interest (ROI) that had a width of $\pm 20^\circ$ from the perpendicular surface point. In the axial direction, the ROI started from 0.1 mm below the cartilage surface and reached to a depth of 1.5 mm. Subsequently, intensity curves of ten cross-sections were averaged. For each scaffold, average μ_t and μ_b were calculated from

the OCT scans that were repeated four times. Each scaffold set included one scaffold with no chondrocytes or collagen (reference scaffold). The μ_t and μ_b values of each scaffold were normalized with those obtained from the reference scaffold prior to statistical analysis. In this way, the possible daily variation in the signal level and the effect of agarose on the optical properties were minimized. Since the scaffolds with 100 mg/ml of collagen were prepared separately from the other scaffolds, there might have been some small differences in their preparation and the measured parameters could not be normalized with the same reference sample properties as the others. Therefore, this set was excluded from the statistical analyses.

μ_t AND μ_b OF THE OSTEOCHONDRAL SAMPLES

In study **II**, the average depth-dependent OCT signal was determined from five adjacent cross-sectional images recorded at the site of interest in the osteochondral samples. The cartilage surface in each image was detected automatically using an optimized threshold and morphological operations, while the tidemark between the non-calcified and calcified cartilage was determined manually. The width of the ROI was set to 21 scan lines (15.2°) and the height was assessed as the distance from the cartilage surface to the tidemark. However, in order to avoid the specular reflection at the cartilage surface, the first 5% of the average curve was excluded from the analysis.

5.5.3 OCT measurement of cartilage thickness

In study **III**, non-calcified and full cartilage thicknesses were measured from the OCT images of the osteochondral samples after careful comparison of the measurement location with the corresponding light microscopy image. The optical path length measured from the OCT image was corrected to respond to the true thickness using the refractive index of cartilage obtained from literature ($n_{cartilage}$ = 1.385 [113]). The same value was used for both non-calcified and

calcified cartilage. Calcified cartilage in the OCT images was seen as a low scattering layer between the non-calcified cartilage and the subchondral bone. This layer was visible in all but three samples.

5.5.4 Determination of speed of sound

Speed of sound

For the determination of SOS in equine cartilage, the thickness and ultrasound TOF were measured from raw OCT and ultrasound images, respectively. An average cartilage thickness within a 1 mm wide window placed under the ultrasound probe was measured by determining the cartilage surface and the tidemark manually. Non-calcified cartilage thickness was used instead of the full cartilage thickness, as the ultrasound reflection is reported to originate from the tidemark [136]. The average thickness in ten adjacent cross-sections was calculated. The average ultrasound TOF was determined from ten subsequently recorded ultrasound images. Each ultrasound A-scan line forming the image was first bandpass filtered (tenth order Butterworth filter, upper cut-off frequency 80 MHz, lower cut-off frequency 15 MHz). Cross-sectional images were constructed from the Hilbert envelopes of the filtered A-scan lines. An average time between the ultrasound reflections from the sample surface and tidemark was measured manually by defining these interfaces in the ultrasound images from as wide an area as feasible. SOS was then calculated as

$$\mathrm{SOS} = \frac{\mathrm{Thickness} \times 2}{\mathrm{TOF}}. \tag{5.6}$$

The SOS in the phantoms was determined similarly.

In arthroscopic measurements of SOS in articular cartilage of human ankle (study **A**), the average thickness of cartilage within a 1 mm wide window was measured after detecting the cartilage surface automatically and the tidemark manually. The window was placed under the ultrasound probe, but when a shadow from the

ultrasound probe prevented the visibility directly below the probe, the thickness measurement was conducted from the adjacent area, as close to the ultrasound probe as possible. Again, the thickness was measured from ten adjacent cross-sections and averaged. Ultrasound TOF was determined from ten subsequently measured A-scan lines perpendicular to the cartilage surface. The Hilbert envelopes of the filtered signals were determined and the TOF between the first arriving signals (50% of the peak) of the surface and tidemark reflections was measured.

Numerical evaluation of the error in speed of sound measurements

The percentage error in SOS caused by the inaccuracy in thickness and TOF measurements depends on the thickness of cartilage. An estimate of the level of error was obtained by calculating the propagation of uncertainty. The estimation of error was conducted in the cases of different cartilage thicknesses by assuming a true SOS of 1615 m/s and allowing the thickness to vary between 0.3 mm and 3.0 mm. The errors arising from the two error sources, thickness and TOF measurements, were separately determined. First, the error in TOF measurement was allowed to vary from 0 µs to 0.050 µs, but the error in thickness measurement was kept negligible. In the second evaluation, the thickness measurement error was varied between 0 µm and 50 µm, and the TOF measurement was assumed to produce no error.

5.5.5 Statistical analysis

The repeatability of the OCT measurements in study **I** was evaluated by calculating intra-class correlation coefficient (ICC). The root mean square coefficients of variation (CVrms(%)) for the repeated measurement of SOS in phantoms and equine cartilage were calculated to determine the reproducibility of the SOS measurements.

Spearman's rank correlation test was used to estimate the relationship between the optical parameters and collagen or chon-

drocyte content of the agarose scaffolds (study **I**), between the optical properties and the structural, compositional and mechanical properties of cartilage samples (study **II**), and between the cartilage thicknesses measured from OCT image and light microscopy image (study **III**).

Kruskal-Wallis test was employed to assess the significance of the differences in the optical properties between the agarose scaffold groups (study **I**) and in the thickness and SOS of cartilage between different anatomical locations (study **III**).

Linear dependences between the SOS and the compositional, structural and biomechanical properties of the osteochondral samples were evaluated by linear mixed model analysis (study **III**). Here, the joint, from which the sample was prepared, was used as the random variable.

The limit for statistical significance in all tests was set to $p < 0.05$. Statistical analyses were conducted using Matlab (2014a; Mathworks Inc., Natic, MA, USA) and SPSS (IBM SPSS Statistics 19, SPSS Inc., Chicago, IL, USA)

Depth-dependent compositional and structural properties and possible degeneration usually starting from the surface of articular cartilage are assumed to cause depth-dependent light backscattering and attenuation. Partial least squares (PLS) regression models [137] were developed between the depth-dependent OCT signal measured from the osteochondral samples in study **II** and the following properties: permeability, fibril network modulus, nonfibrillar matrix modulus and the Mankin score at the site of interest, and OD, absorbance in Amide I region and collagen orientation in whole cartilage and in superficial zone (10% of cartilage thickness), transitional zone (15%) and deep zone (75%). The PLS method is used to find the relation between the predictor and response by searching those features of the predictor variable that best predict the response variable, *i.e.* the PLS components [137]. The second derivative of the smoothed (fourth degree Savitzky-Golay filter) depth-dependent OCT signal served as the predictor whereas the other properties of the samples were the response variables.

The number of PLS components used in the models was optimized using the leave-one-out cross-validation approach [138]. To avoid over-fitting, the minimum numbers of components providing the highest possible coefficient of determination (R^2) and the lowest possible root mean square error of the cross-validation (RMSECV) were selected for incorporation into the models. In the leave-one-out cross-validation approach, each sample is left out on one occasion from the model development and the other samples are used to predict the response property of the sample omitted. RMSECV was calculated from the deviation of true and predicted response variable value ($\widehat{y}$ and y, respectively) as

$$\text{RMSECV} = \sqrt{\frac{\sum_{i=1}^{N}(\widehat{y}_i - y_i)^2}{N}}, \tag{5.7}$$

where subscript i indicates the sample and N is the number of samples. After obtaining the optimal model, the properties of all samples were predicted using the optimal model and the root mean square error of this prediction (RMSEP) was calculated. PLS analysis was conducted by utilizing the SIMPLS algorithm in Matlab.

6 Results

6.1 OCT ARTHROSCOPY OF HUMAN JOINTS

Arthroscopic OCT imaging was found equally applicable in both large (knee, ankle, elbow, and wrist) and small (MTP1 and MCP1) joints in study **A**. Injuries and degeneration of articular cartilage, such as holes, fissures, and fibrillation, were detected in the OCT images (Figure 6.1). In some OCT images, bright spots or irregular scattering within cartilage were detected (Figures 6.1b and 6.1g). Irregular scattering is assumed to indicate a degeneration of collagen network, and the bright spots may be caused by cuts or abnormal content of the tissue structural components.

OCT enabled the measurement of width and depth of the lesions and thickness of articular cartilage up to about 1.5 mm. Wearlines in the cartilage of an ankle were seen with conventional arthroscopy and OCT. Based on the arthroscopic image, the surgeon estimated their ICRS grade to be 3-4. However, the OCT image revealed that the cartilage thickness was high and the lesion did not exceed 50% of the thickness. Thus, the ICRS grade 2 was awarded based on the OCT image.

In the elbow, cartilage on capitulum appeared to be completely intact in conventional arthroscopy, but displayed evidence of minor local wear in OCT image. Additionally, a severe cartilage fissure was found from a narrow space between capitulum and radius (6.1c). Without OCT, this lesion would have not been detected, because it was impossible to access this location with a conventional arthroscope.

In MTP1, a crack reaching the cartilage-bone interface was detected in the OCT image (Figure 6.1d). This lesion was completely missed in the conventional arthroscopy, although the joint was diagnosed as being osteoarthritic.

Due to the small size of the MCP1, OCT imaging of this joint was performed without arthroscopic guidance. Despite the diffi-

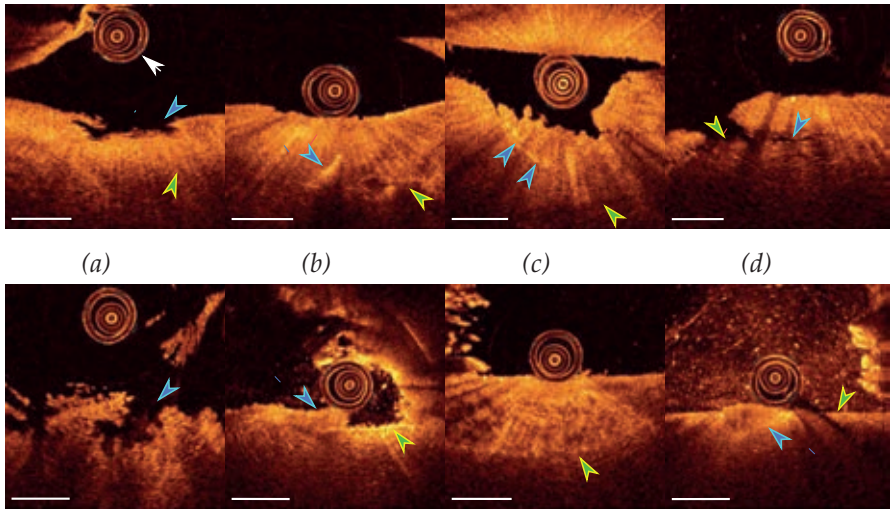

Figure 6.1: Arthroscopic OCT imaging enabled visualization of (a) holes and (b) bright spots in cartilage, (c)-(d) fissures, (e) fibrillation, (f) wear and absence of cartilage, (g) irregular scattering within cartilage, and (h) abnormality of exposed subchondral bone. White arrow in (a) indicates the OCT probe seen in the image. The blue and the green arrows mark the interesting structural features and the approximate location of the subchondral bone interface, respectively. The scalebar equals 1 mm at refractive index of 1.33.

culties in positioning without any arthroscopic assistance, severe osteoarthritis in the joint was detected. In practice, there was no cartilage left on the subchondral bone, and a bone abnormality was seen (Figure 6.1h).

At first sight, significantly different diagnoses for wrist joint were obtained with conventional arthroscopy and OCT. Based on the arthroscopic image, the surgeon estimated that the cartilage on the radial surface had completely worn out, whereas the OCT image showed that there was about a 1 mm thick cartilage layer. The discrepancy in the diagnoses was an important finding, as it enabled the surgeon to acknowledge the possibility of false diagnosis and thus to conduct a more comprehensive evaluation of the joint. With palpation and more extensive OCT scanning, the wearing of

cartilage was found to be local although in the arthroscopic image, the appearance of the whole joint was uniform.

The evaluation of the depth of the cartilage lesion was easier by means of ultrasound and OCT imaging than with conventional arthroscopy. There were many times when the estimation of the severity of cartilage degeneration (qualitative estimation or ICRS scoring) that had been assessed by both palpation and conventional arthroscopy imaging was made more detailed or the assessment was changed after OCT imaging.

Compared to ultrasound, OCT provided more detailed images of the lesions (Figure 6.2). Minor wear and fibrillation were easier to detect with OCT, while ultrasound imaging was superior in the visualization of the cartilage-bone interface when the thickness of cartilage was high. However, the imaging of cartilage-bone interface was improved by OCT in those cases with thin and fibrillated cartilage.

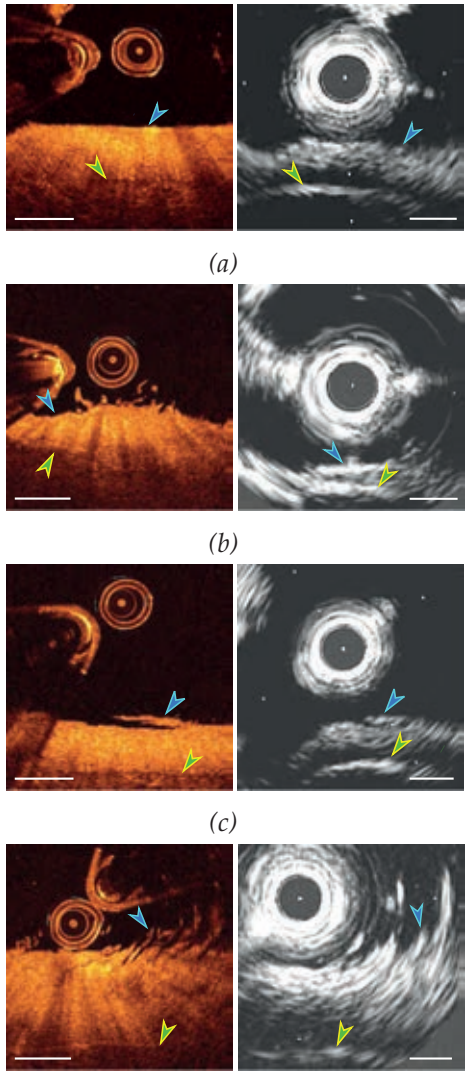

(a)

(b)

(c)

(d)

Figure 6.2: Simultaneously recorded OCT (on the left) and ultrasound (right) images of (a) intact articular cartilage, (b)-(c) mild fibrillation, and (d) severe fibrillation. The blue arrows indicate the cartilage surface or the lesion and the green arrow the bone interface. The scalebar in OCT images equals 1 mm at refractive index of 1.33 and in ultrasound images 1 mm at a speed of sound 1636 m/s.

6.2 LIGHT ATTENUATION AND BACKSCATTERING IN AGAROSE SCAFFOLDS AND ARTICULAR CARTILAGE

In study **I**, the elevation in the collagen concentration or chondrocyte density in the agarose scaffolds increased light attenuation and backscattering (Figure 6.3). The correlations of μ_t and μ_b with collagen content were $\rho = 0.694$ ($p < 0.001$) and $\rho = 0.103$ ($p = 0.422$), respectively. The corresponding correlations with chondrocyte density were $\rho = 0.853$ ($p < 0.001$) and $\rho = 0.504$ ($p < 0.001$).

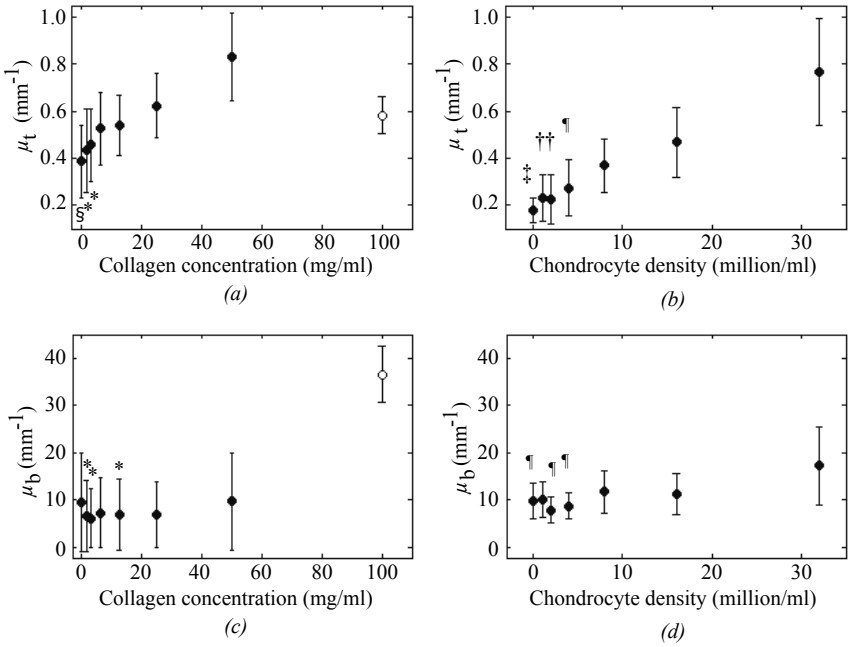

*Figure 6.3: Total attenuation coefficient (μ_t; mean ± SD) of the agarose scaffold as a function of (a) collagen concentration and (b) cell density in the scaffolds. (c) The backscattering coefficient (μ_b) as a function of collagen concentration and (d) as a function of chondrocyte density of the scaffolds. Results within scaffolds with significantly different values ($p < 0.05$) compared to scaffolds with 25-50 mg/ml of collagen, 50 mg/ml of collagen, 8-32 million chondrocytes per milliliter, 16-32 million chondrocytes per milliliter and 32 million chondrocytes per milliliter are marked with §, *, ‡, †, and ¶, respectively.*

Thus, light attenuation was more sensitive to changes in the number of scattering particles than backscattering coefficient. The ICC values for the repeated μ_t and μ_b measurements were 0.951 and 0.973, respectively.

Light microscopy imaging and FTIR spectroscopy were conducted in order to confirm the composition of the prepared agarose scaffolds. The microscopy images of the stained sections prepared from the scaffolds showed systematic relative increase in chondrocyte density and almost uniform distribution of chondrocytes or collagen (Figure 6.4). However, local chondrocyte or collagen clusters were detected in a few sections. The expected increase in collagen concentration in the scaffolds was verified with FTIR measurements (Figure 6.5).

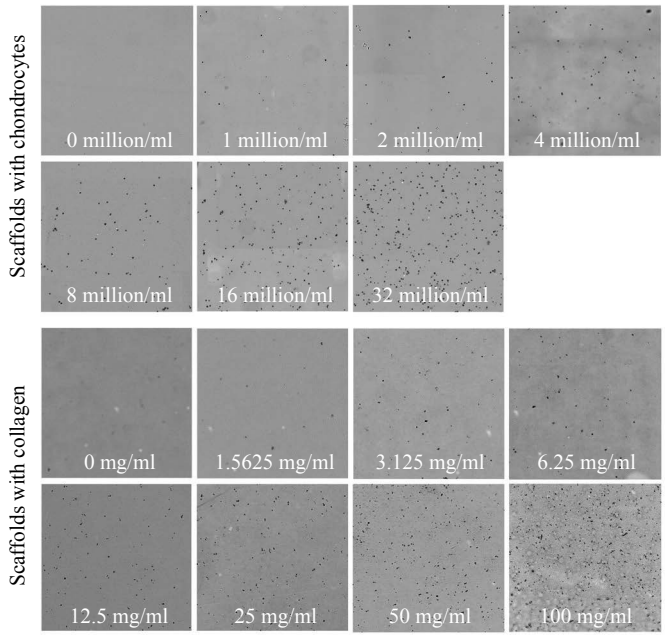

Figure 6.4: Light microscopy images of the representative agarose scaffolds with varying amount of chondrocytes or collagen. Chondrocyte samples were stained with hematoxylin and eosin, and the collagen samples with Masson's trichrome. The image widths in upper and lower two rows are 1 mm and 0.5 mm, respectively.

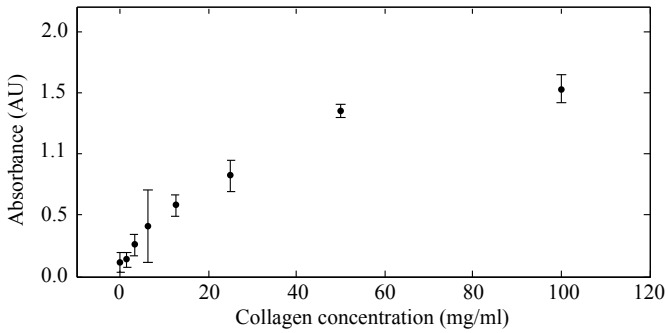

Figure 6.5: Light absorbance in amide I region in agarose scaffolds with varying amount of collagen.

Light attenuation and backscattering in equine articular cartilage were measured in study **II**. Mean (SD) μ_t and μ_b of the equine articular cartilage were 2.2 mm^{-1} (1.1 mm^{-1}) and 13.4 mm^{-1} (7.9 mm^{-1}), respectively. A weak, but statistically significant correlation was found between the fibril network modulus of samples and their light backscattering property ($\rho = 0.280, p = 0.03$). However, the bulk measures of light backscattering and attenuation, μ_b and μ_t, respectively, did not correlate significantly with the other determined properties of articular cartilage $p > 0.05$.

Table 6.1: Spearman's rank correlation coefficients between the total attenuation and backscattering coefficients and the measured compositional, structural and biomechanical properties of articular cartilage.

	Mankin score	Permeability	E_m	E_f	OD	Absorbance in 1594-1720 cm^{-1}	Collagen orientation
μ_t	0.019	-0.043	0.107	0.093	-0.021	0.071	0.129
μ_b	-0.026	-0.128	0.166	0.280*	0.086	0.241	0.136

μ_t = total attenuation coefficient, μ_b = backscattering coefficient, E_m = non-fibrillar matrix modulus, E_f = fibril network modulus, OD = optical density, * $p \leq 0.05$.

In study **II**, PLS regression analysis was applied to relate the complete depth-dependent OCT signal to the compositional, struc-

tural and biomechanical properties of articular cartilage. For the PLS models, three to seven components were chosen based on the optimal RMSECV and R^2 in crossvalidation (Table 6.2). The properties of cartilage samples were predicted with the developed models. The predictions of Mankin score, permeability, OD, and collagen orientation were the most successful ($R^2 \geq 0.70$; Table 6.2). The predictions of OD and light absorbance in the amide I region were notably improved by predicting the properties of the superficial, transitional and deep zones separately. All the samples with no to mild degeneration were correctly classified into this category after PLS prediction of the Mankin score. There were nine samples having moderate to severe degeneration; six were correctly classified.

6.3 OCT MEASUREMENT OF CARTILAGE THICKNESS

Non-calcified cartilage and full cartilage thicknesses were successfully measured from the equine osteochondral samples in study **III**. The correlations between the thicknesses measured from OCT and light microscopy images were $\rho = 0.916$ ($p < 0.001$) and $\rho = 0.845$ ($p < 0.001$) for non-calcified and full cartilage thickness, respectively (Figure 6.6). The average full cartilage thickness was 1.00 mm (SD = 0.26 mm), while the maximum measurable full cartilage thickness with OCT was 1.8 mm. The corresponding values for non-calcified cartilage were 0.83 mm (SD = 0.25 mm) and 1.44 mm, respectively. The thickness of non-calcified cartilage in P1 (mean $\pm$ SD = 1.03 mm $\pm$ 0.27 mm) was significantly higher than in SR (0.74 mm $\pm$ 0.16 mm, $p = 0.001$) or MC3 (0.71 mm $\pm$ 0.13 mm, $p < 0.001$). The layer of calcified cartilage was not discernible in OCT the images of three samples due to excessive light attenuation.

6.4 SPEED OF SOUND MEASURED WITH COMBINED OCT AND ULTRASOUND IMAGING

SOS in phantom materials measured with the developed arthroscopic technique and with the reference technique are presented in

Table 6.2: Mean of the measured properties of articular cartilage and the statistical evaluation of the PLS prediction of the properties based on the depth-dependent OCT signal.

Property	Zone	Mean (SD)	N_{comp}	RMSEP	R^2
Mankin score	All	3.5 (2.6)	5	1.4	0.70
Permeability ($\times 10^{-15}$ m^4/(Ns))	All	5.5 (8.7)	5	4.4	0.74
E_m (MPa)	All	0.25 (0.24)	3	0.17	0.50
E_f (MPa)	All	1.74 (1.18)	3	0.89	0.42
OD (AU)	All	1.42 (0.37)	5	0.16	0.73
	Superficial	0.67 (0.40)	6	0.18	0.79
	Transitional	1.20 (0.55)	6	0.25	0.79
	Deep	1.57 (0.35)	6	0.16	0.80
Absorbance in 1594-1720 cm^{-1} (AU)	All	42.0 (4.9)	4	3.7	0.43
	Superficial	23.6 (4.6)	5	2.7	0.64
	Transitional	30.7 (5.0)	5	3.2	0.57
	Deep	46.7 (5.3)	5	8.8	0.56
Collagen orientation (°)	All	66.2 (14.4)	7	7.1	0.75
	Superficial	35.9 (17.0)	4	11.3	0.55
	Transitional	58.7 (16.1)	4	10.6	0.56
	Deep	71.7 (16.8)	4	11.8	0.50

SD = standard deviation, N_{comp} = number of PLS components, RMSEP = root mean square error in prediction, R^2 = coefficient of determination, E_m = non-fibrillar matrix modulus, E_f = fibril network modulus, OD = optical density.

Table 6.3 (study **III**). The correlation between the two techniques was statistically significant ($\rho > 0.99$, $p < 0.001$). The value of CVrms(%) of the measurements conducted with the arthroscopic technique was 3.4%.

The average SOS in equine articular cartilage measured with the developed arthroscopic technique was 1636 m/s (study **III**). SOS was not significantly dependent on the anatomical location

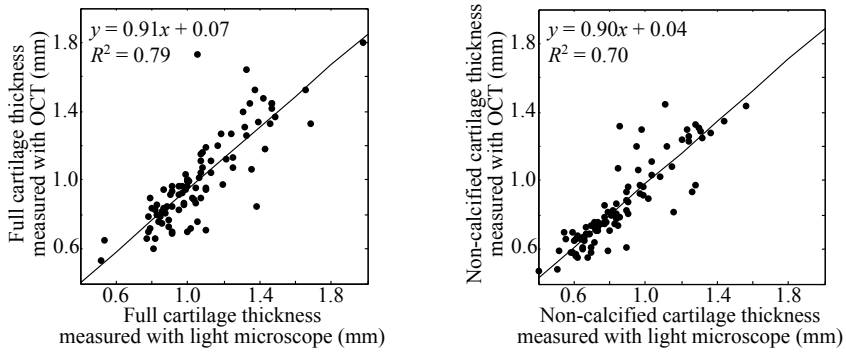

Figure 6.6: Thickness of (a) full cartilage and (b) non-calcified cartilage measured with OCT and light microscopy.

Table 6.3: Speed of sound in phantom materials measured with the two studied techniques.

	silicone	4% agarose	2% agarose	ABS	glass
Arthroscopic technique (m/s)	1017	1352	1391	2871	5453
Reference technique (m/s)	1021	1300	1363	2747	5671

ABS = Acrylonitrile butadiene styrene

($p = 0.284$). CVrms(%) for the repeated measurements of SOS was 7.8%. When the variations in cartilage thickness and ultrasound TOF measurements were separately investigated, CVrms(%) values of 7.3% and 7.6%, respectively, were obtained. There was no statistically significant linear dependence observable between the SOS in equine articular cartilage and the compositional, structural, or biomechanical properties of articular cartilage (Table 6.4).

In study study **A**, the arthroscopic applicability of the developed technique for measurement of SOS in articular cartilage was tested in a human cadaver ankle. It was found that it was possible to conduct a successful arthroscopic SOS measurement. The mean

Table 6.4: p-values for linear mixed model association between speed of sound (dependent variable) and compositional, structural, and biomechanical properties of articular cartilage (fixed variables).

Fixed variable								
Mankin score	OD	Collagen orientation	PI	PG content	Collagen content	E_f	E_m	k
0.521	0.771	0.421	0.924	0.844	0.355	0.381	0.528	0.449

Linear mixed model analysis. Significant dependence ($p < 0.05$).
OD = optical density, PI = parallelism index, PG = proteoglycan, E_f = fibril network modulus, E_m = non-fibrillar network modulus, k = permeability.

SOS in the articular cartilage of the human ankle was 1564 m/s (SD = 239 m/s).

The numerically analyzed levels of error in SOS measurements for cases of varying accuracy in thickness and TOF measurements and varying thickness of cartilage are presented in Figure 6.7.

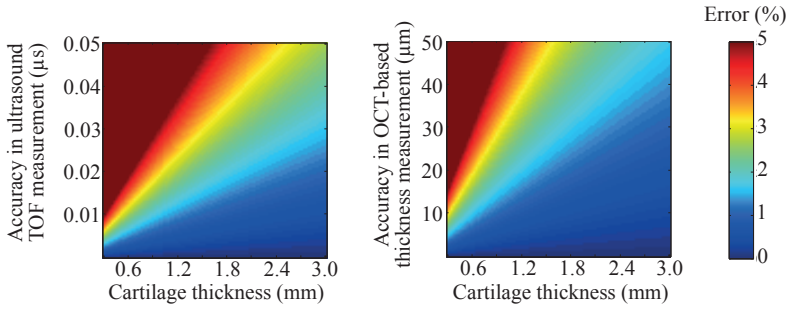

Figure 6.7: Numerical evaluation of the measurement error in the determination of SOS for cartilage with different thicknesses in cases of variable accuracy in TOF or thickness measurements.

6.5 EVALUATION OF CARTILAGE REPAIR

In study **B**, the repair tissues could be readily recognized from OCT and ultrasound images immediately after the repair (Figure 6.8, Timepoint 1). The fibrin glue applied in repair technique 1

showed high and low ultrasound scattering areas. The same inhomogeneous feature was detected in OCT images. GelMA with equally spread cells (technique 2) had a uniform and high ultrasound and light scattering structure, and the interface of the repair tissue and surrounding cartilage was clearly visible in the ultrasound and OCT images. In repair technique 3, the cells were placed on the bottom of the defect and covered with GelMA. The plain GelMA produced small scattering of ultrasound, and therefore it was difficult to observe the tissue in the ultrasound images. However, when the cell-free GelMA was injected onto the cell layer, it was noted that some of the cells had spread towards the interface between the repair tissue and the defected cartilage. The high cell number close to the interface compared to the center of the defect was determined via its high ultrasound and intense light scattering. The PCL scaffolds in GelMA (repair technique 4) were readily detected in both OCT and ultrasound images. Due to high ultrasound and light scattering in PCL scaffolds, this was the only repair tissue type through which the microfractures performed on to the subchondral bone were difficult to visualize with OCT and ultrasound imaging. The filling of the defect was easier to estimate from OCT than from ultrasound images due to its higher resolution.

After two months of healing, the defect sites were again imaged, first with conventional arthroscopy and then with OCT and ultrasound. The arthroscopic images reveiled that the tissue had grown on all of the defects, and this was estimated to be fibrocartilage (Figure 6.8, Timepoint 2). The drilled defects were no longer completely filled with the repair material or tissue. From the arthroscopy image, it was not possible to evaluate the thickness of the fibrous tissue layer or the presence of the implanted material under the fibrous tissue. The thickness of the layer, however, could be estimated from the OCT images; it was found to be thin, only about 100-300 µm at all the imaged sites. The fibrous tissue scattered more light and ultrasound than the implanted materials. There was seen no sign of any material which would be optically different from fibrous tissue. Therefore, it is assumed that the implanted materials

have drifted away from the implanted sites, or possibly worn away or simply been degraded. This will be verified in later histological analyses. When evaluated from the OCT images, the surface of the

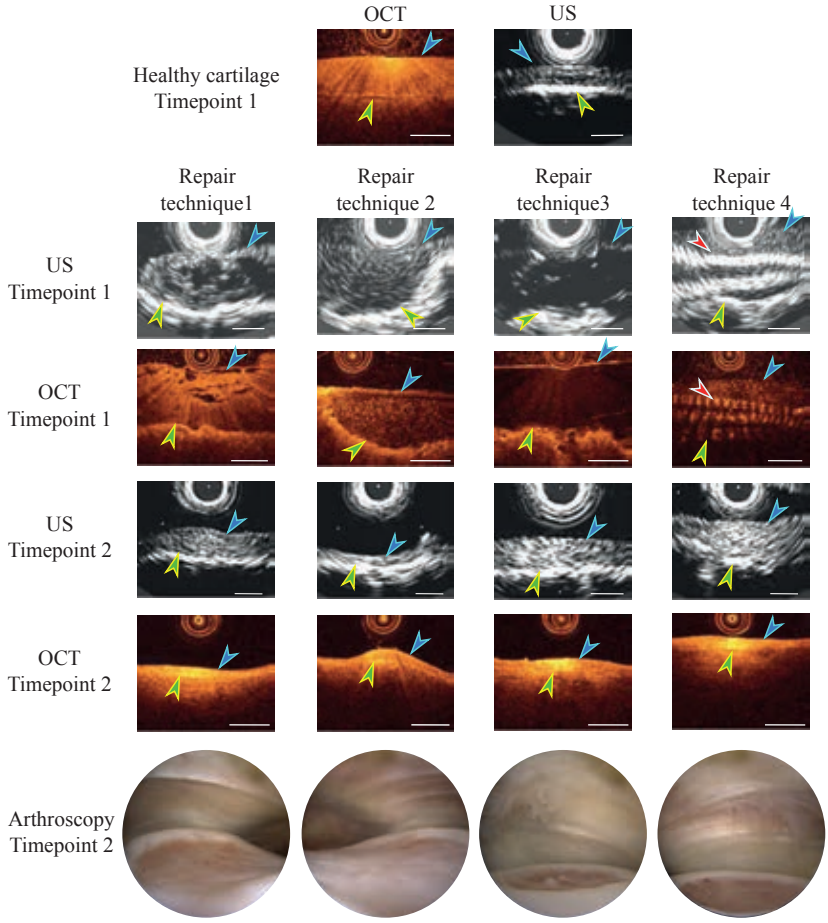

Figure 6.8: OCT and ultrasound images of healthy cartilage and the articular cartilage defects immediately after the repair (timepoint 1), and images of the defects after two months of healing (timepoint 2). Four different repair techniques were tested. Arthroscopic images of the repaired defects on timepoint 2 are shown in the bottom row. The blue, green, and red arrows mark the tissue surface, bone-interface, and the PCL scaffold, respectively. The scalebar in OCT images equals 1 mm at refractive index of 1.33 and in ultrasound images 1 mm at speed of sound 1636 m/s.

surrounding cartilage was still intact in most of the cases. Some minor evidence of wear was seen only around four defects, which had all been repaired with different techniques.

None of the repair techniques showed any additional kind of healing other than the growth of fibrous tissue. Thus, based on OCT or ultrasound evaluations, none of the repair techniques can be regarded as superior to any of the others. The defects are to be imaged again six and twelve months after the procedure. The biological nature of the tissue which has grown in the defects will be analyzed by histology and biochemical assays.

7 Discussion

In arthroscopic joint repair surgery, the integrity of articular cartilage is routinely evaluated by means of visual investigation and palpation of the articulating surfaces. However, these techniques have been reported to be highly subjective and poorly repeatable [20]. OCT may be more sensitive than conventional arthroscopy in its ability to detect of small or subsurface lesions and early cartilage degeneration [97, 139]. Furthermore, OCT could provide quantitative information on the composition, structure and degenerative stage of articular cartilage. This thesis consists of substudies **I-III** and previously unpublished studies **A** and **B**, which investigated the feasibility of using arthroscopic OCT in imaging of articular cartilage, such as in the detection of articular cartilage degeneration and in the evaluation of the success of cartilage repair surgery.

Study **A** investigated the applicability of a commercial intravascular OCT system in arthroscopic imaging of cartilage in small and large human joints. The effect of composition and structure of articular cartilage on the measured OCT signal was assessed in studies **I** and **II**. Furthermore, OCT imaging with simultaneous ultrasound imaging was employed in the measurement of the SOS in articular cartilage, which is known to change due to degeneration. For this purpose, an arthroscopically applicable technique was developed, combining simultaneous measurement of ultrasound traveltime through cartilage and OCT-based measurement of cartilage thickness and this way tested in study **III**. Prior to this, the accuracy of the OCT in the measurement of articular cartilage thickness was evaluated. Finally in study **B**, OCT was used *in vivo* to evaluate the success of the surgical repair of damaged articular cartilage.

7.1 ARTHROSCOPIC USE OF OCT

Arthroscopic OCT imaging has been conducted in porcine and equine joints [22, 26, 96] and in human knee and first carpometa-

carpal joints [97–100]. For the first time, the feasibility of using arthroscopic OCT imaging of human ankle, elbow, wrist, MTP1, and MCP1 joints was evaluated in study **A**. Arthroscopic OCT imaging of articular cartilage was assessed as being feasible in both the large and small human joints. The probe was inserted into the joint through a custom-made instrument channel or the instrument channel of the arthroscope. The guiding of the imaging probe was straightforward when the joint was simultaneously imaged with an arthroscope.

OCT provided high resolution images of cartilage and visibility to subchondral bone in locations with cartilage thickness of less than about 1.5 mm. Both small lesions and wear of the cartilage surface were easily detected. The evaluation of the depth of the lesion was easier based on OCT than from the conventional arthroscopy image, because arthroscopy enables only an assessment of the cartilage surface. Consequently, it was determined that it was easier to use the OCT image than conventional arthroscopy to evaluate the ICRS scoring, which is based on the evaluation of the lesion depth with respect to cartilage thickness. In a later study by te Moller *et al.* (2013), it was claimed that there was a poor agreement between the ICRS scores for the lesions based on OCT and arthroscopic images, and as in study **A**, OCT provided more detailed information about the lesions than could be obtained with conventional arthroscopy [22]. Furthermore, the Degenerative Joint Disease (DJD) classification made based on OCT images has been found to match well with the microscopic assessment of DJD [140], and the reproducibility of the OCT-based ICRS scoring has been reported as being better than that of the scoring based on conventional arthroscopy [96].

It is believed that OCT is more sensitive at detecting minor cartilage wear than conventional arthroscopy [98]. In comparison to ultrasound, OCT provides a more detailed image of the lesions, but the cartilage-bone interface can usually be better visualized with ultrasound.

Arthroscopically inaccessible, narrow areas may be accessible with a small OCT probe [22, 96]. In study **A**, a lesion in elbow

cartilage was detected with OCT at a location difficult to image with a conventional arthroscope. Unfortunately, the fragility of the OCT probe prevented imaging of the areas where there was a risk that the probe would be crushed. The OCT system used in this thesis work was chosen due to the small diameter of the imaging probe. Because of the rotating fiber optics the catheter is very fragile and prone to distortions should it be bent or rotated. This could be avoided using a translation device instead of the rotating device.

7.2 SENSITIVITY OF OCT TO DETECT CHANGES IN THE CHARACTERISTICS OF ARTICULAR CARTILAGE

Studies with agarose scaffolds

The measurement of total attenuation coefficient with OCT makes it possible to conduct a quantitative tissue characterization. The differences in attenuation coefficients in tissues are attributable to variations in the compositional or structural properties and this may help in the detection of tissue pathologies [141–143]. For example, different atherosclerotic plaque types exhibit different types of light attenuation [144,145]. The backscattering coefficient could also have value in tissue characterization [24].

The progressive degeneration of articular cartilage is attributable to alterations in tissue compositional and structural properties, like changes in chondrocyte content and a decrease in collagen content. Although the number of studies investigating the applicability of quantitative OCT in the evaluation of articular cartilage integrity is increasing, the contribution of the individual structural components of the tissue to the OCT image has not been thoroughly studied. Study **I** used OCT to assess the total attenuation and backscattering coefficients of agarose scaffolds with varying chondrocyte and collagen contents. Light attenuation and backscattering in agarose scaffolds were significantly increased with the increasing collagen or chondrocyte content in the scaffolds. The higher sensitivity of attenuation coefficient compared to backscattering co-

efficient on the composition changes is a result of high forward scattering in turbid material [93]. The results of study **I** suggest that especially the attenuation coefficient but also the backscattering coefficient could be potentially useful parameters for monitoring compositional changes in engineered biomaterials.

Enzymatic degradation of collagen network has been found to reduce light scattering from the most superficial layer of articular cartilage, whereas the trypsin digestion of proteoglycans did not affect the superficial OCT signal [103]. Bear *et al.* (2010) observed a decrease in backscattering at a depth range of 232-300 µm and an increase of scattering at the depth range of 33-100 µm in bovine cartilage after an impact with sufficient energy to cause cell death, but no visually observable damage [107]. According to the previous studies and study **I** of the present thesis, OCT has the potential to reveal compositional and structural changes in engineered material or cartilage. However, the total attenuation and backscattering coefficients obtained in study **I** cannot be directly compared to those measured from the native cartilage. Articular cartilage has multiple components and different structural features like collagen orientation and crosslinking which all affect its optical properties.

Total attenuation and backscattering coefficients were found to increase nonlinearly in conjunction with the increases in collagen and chondrocyte contents. This nonlinearity of the relations is assumed to follow from multiple and dependent scattering [146]. In many studies, the single scattering model has been used to describe the light propagation in soft tissues [24, 144]. The single scattering model has been found to be valid for low scattering materials ($\mu_t <$ 6 mm^{-1}) like those used in studies **I** and **II** [133, 147]. Where applicable, the single scattering model is preferred over the multiple scattering model because of its simplicity.

The agarose scaffolds with collagen content of 100 mg/ml deviated from the other samples. Their backscattering coefficient was high as could have been expected, but the attenuation coefficient was low. The reason for the low attenuation coefficient could not be identified.

Studies with osteochondral samples

In study **I**, major differences in the collagen and chondrocyte contents between the agarose scaffolds were needed to reveal statistically significant differences in the optical properties. However, the changes in cartilage composition in OA or as a result of an injury may be relatively small. Study **II** investigated the relationship of the compositional, structural, and biomechanical properties to the total attenuation and backscattering coefficients of equine articular cartilage. The mean total attenuation coefficient in the cartilage samples was 2.2 mm^{-1}, which is lower than the mean attenuation coefficient for goat cartilage assessed in a previous study (8.2 mm^{-1} [25]). The goat cartilage was healthy, whereas in this thesis, the sample set included osteoarthritic and injured samples in addition to healthy specimens. The difference in the total attenuation or backscattering coefficients of healthy and degenerated articular cartilage has not been previously studied, but the attenuation coefficient of spontaneously repaired tissue has been found to be significantly lower than that of the native cartilage [25]. However, the optical attenuation index, a parameter describing the strength of the attenuation, was found to be insensitive to early-to-moderate cartilage degeneration [148].

Study **II** did not reveal any statistically significant correlations in the comparison of the total attenuation and backscattering coefficients and compositional, structural, and biomechanical properties of equine cartilage. Total attenuation and backscattering coefficients are bulk values for the tissue. Articular cartilage is a layered material, and degeneration does not present itself equally throughout the depth of cartilage. Additionally, there are many varied and complex compositional and structural changes related to cartilage degeneration and their summed effect on the light propagation in the tissue is difficult to estimate. Thus, the bulk measures for attenuation and backscattering may not optimally represent articular cartilage.

Following the poor correlation between the attenuation and backscattering coefficients and the measured properties of articular cartilage, a PLS approach was employed in study **II** as an alternative analytical method. The advantage of the PLS regression is that it takes into account the depthwise variation of the OCT signal by considering the OCT signal as a multivariate input, where the amount of light backscattering from each depth forms one variable. PLS regression analysis attempts to include the most informative features of this multivariable input into the model. The objective is to predict most of the variation in the response variable values (in study **II** the compositional, structural, or biomechanical property to be predicted) based on the selected features of the OCT signals [137].

Optical density (*i.e.* fixed charge density), permeability, mean collagen orientation, and Mankin score predicted with the developed PLS models displayed a high correlation with the measured values. The correlations for non-fibrillar matrix modulus, fibril network modulus and collagen content evaluated by FTIR were lower. In previous studies, the contribution of proteoglycans to the OCT signal has been negligible [103, 149]. However, these studies investigated the influence of proteoglycans to birefringence and scattering at the surface of the tissue instead of depth-dependent backscattering. The contribution of proteoglycans to OCT light backscattering is of great interest, because a reduction in the proteoglycan content is one of the earliest signs of degeneration [150, 151]. Proteoglycans regulate the permeability of articular cartilage [29]. Thus, the good correlation between the measured and predicted permeability may result from the contribution of proteoglycans.

Although the OCT system used in this thesis is not designed for the measurement of polarization properties of the tissue, the collagen orientation in cartilage has a small effect on the OCT signal. The relation of collagen orientation and the birefringence properties of articular cartilage is well known [28, 152, 153]. Detailed information about the birefringence properties can be obtained with a PS-OCT system [23, 109, 111].

Mankin score describes the overall integrity of articular cartilage. In the determination of the Mankin score, the cartilage structure, the tissue cellularity and the proteoglycan content are all separately assessed and the final score is a sum of the sub-scores [125]. The chondrocyte and proteoglycan contents, together with the collagen network, have been assumed to be the main features that influence the OCT signal.

The correlation between the measured and predicted FTIR absorbance in amide I region, *i.e.* the collagen content, was low. Based on the results in studies **I** and **II**, it seems that the OCT signal is less sensitive to alterations in collagen content than that in chondrocyte content. In OA, the orientation of the collagen network usually changes before there is any reduction in the collagen content [5], and can be detected with PS-OCT. Thus, the detection of changes in collagen content may not be so important for the diagnosis of early stage degeneration.

Multivariate analysis of OCT signal may have the potential to assist in the characterization of articular cartilage. However, in study **II**, the developed models were not validated with an independent test set. The proper validation of the models would be important before drawing any further conclusions of their validity. Thus, a further study with a larger test set is warranted.

7.3 SUITABILITY OF OCT FOR MEASUREMENT OF ARTICULAR CARTILAGE THICKNESS

OCT has been successfully used for measurement of the thickness of thin rabbit and goat cartilage [25, 112, 154]. It is known that the light penetration depth in soft tissues is limited to about 2 mm at the wavelengths used in OCT imaging [155]. However, the accuracy of the measurement of articular cartilage thicknesses exceeding 0.7 mm has not been previously investigated. In study **III**, osteochondral samples having mean cartilage thickness of 1 mm were imaged with OCT. The cartilage thicknesses measured from the OCT images were compared to the measurements conducted from light

microscopy images. In most of the OCT images of the equine osteochondral samples, the calcified layer was seen as a dark band between the non-calcified cartilage and the subchondral bone. The good detectability of the calcified layer meant that it was possible to make separate measurements of non-calcified cartilage and full cartilage thicknesses. The OCT-measured thicknesses were in line with those measured from light microscopy images. The relative differences between the OCT and microscopy measurements were similar to those obtained for thinner samples in previous studies [25, 112, 154]. In study **III**, the maximum measurable full cartilage thickness was found to be 1.8 mm.

The OCT measurement of articular cartilage thickness requires an estimation of the cartilage refractive index. Correct refractive index is essential, as it is used to transform the measured optical thickness into geometrical thickness. Refractive indices from 1.385 to 1.510 have been used or alternatively the value has been measured for articular cartilage [25, 112, 113, 154]. Degeneration has not been found to have significant effect on refractive index [113]. A value of 1.385 measured for bovine cartilage was used in study **III**. The same refractive indices were used for non-calcified and calcified cartilage, although their composition is different and, therefore, also the true refractive indices may be different. The refractive index of cartilage varies with depth [113], and the refractive index of calcified cartilage warrants for further investigation.

7.4 MEASUREMENT OF SPEED OF SOUND WITH COMBINED OCT AND ULTRASOUND IMAGING TECHIQUE

The speed of ultrasound in articular cartilage depends on the integrity of the tissue. Myers *et al.* (1995) measured about a 5% decrease in SOS due to OA [156]. These investigators found no relationship between the water content and SOS, but later studies have revealed that the reduction in SOS is related to the proteoglycan loss and disruption of collagen network [71, 73, 157], and also to the increase in the water content [158]. Consequently, SOS could

serve as an indicator of OA.

Measurement of SOS requires an accurate estimation of cartilage thickness in addition to the measurement of sound travel time through cartilage. Previously, a combination of ultrasound and MRI has been suggested as being advantageous for the measurement of SOS [159]. However, the resolution of MRI and the accuracy in matching the MRI measurement location with the ultrasound measurement may not be clinically sufficient for detecting local and early stage degenerative changes.

In study **III**, OCT was employed in the measurement of thickness of articular cartilage simultaneously with ultrasound measurement of TOF in cartilage for determination of SOS. An instrument channel was designed to allow the insertion of small OCT and ultrasound probes into the joint. The imaging heads of the probes were kept adjacent, so that the same location could be imaged simultaneously with ultrasound and OCT. As the ultrasound probe was visible in the OCT images, matching of the measurement site was straightforward. Cartilage thickness and ultrasound TOF in cartilage were determined from the OCT and ultrasound images, respectively. The technique was found to be promising when it was tested in the arthroscopic examination of a human cadaver ankle (study **A**).

A good match was obtained between known and measured SOS values in phantom materials. Furthermore, the mean SOS (1636 m/s) measured for equine articular cartilage samples agreed with the value reported in the literature (1696 m/s [160]). The mean SOS measured for the human ankle cartilage (1564 m/s) was also in agreement with the literature, *i.e.* a mean SOS of 1658 m/s and 1581 m/s for healthy and degenerated human cartilage, respectively [156]. However, in contrast to the literature [71,73,157], SOS in equine cartilage was not significantly related to the compositional, structural, and biomechanical properties of the samples.

The poor correlations between the SOS and cartilage structural and biomechanical characteristics may result from the depth dependence of cartilage refractive index and SOS [113,161]. However,

the main reason for the poor correlations is considered to be the insufficient accuracy of the bulk SOS measurements. First, the imaging probes were hand-held during the measurements to mimic the arthroscopic conditions. The angle between the ultrasound beam and the surface of the cartilage was optimized by maximizing the strength of the reflection from the interface. The stability of the instrument became an important factor in the beam orientation. However, in the future it should be possible to avoid this issue by changing the design of the instrument, for example so that it would be positioned on the cartilage such that the incidence angle of ultrasound would be automatically perpendicular to the surface. Second, in many samples, the ultrasound reflection either from the cartilage surface or the bone was too weak to be recognized from a single A-scan line. Due to the rotating imaging geometry, the subsequently recorded A-scan lines were aligned at a different angle and, hence, could not be averaged to improve the signal-to-noise ratio. Therefore, the interfaces were determined manually from the images constructed from the A-scan lines, which is not as accurate as it would be to locate the reflections automatically from the averaged A-scan lines.

The small inaccuracy in either TOF or thickness measurement is exacerbated when the cartilage is thin, as is the case in the present equine joints. For example, if the true SOS is 1615 m/s and the cartilage thickness is 1.5 mm, then a TOF measurement error equal to the wavelength produces about a 3% error in the SOS measurement. In contrast, for cartilage with a thickness of only 0.5 mm, the error would be about 8%. It was estimated that a 20 μm inaccuracy in the thickness measurement would produce errors of about 1% in 1.5 mm cartilage and 4% in 0.5 mm cartilage, respectively.

7.5 OCT IN THE EVALUATION OF SURGICAL CARTILAGE REPAIR

In earlier studies, OCT has been used to measure the surface roughness, optical surface reflection, light backscattering, and area of

spontaneously repaired tissue *in vitro* [25, 104]. Additionally, it has been found that OCT could be used *in vitro* to monitor the integration of tissue-engineered implants with cartilage [162]. However, this has not been verified *in vivo*. Study **B** was conducted in order to investigate the use of arthroscopic OCT in the evaluation of the success of cartilage repair surgery. During the two months of healing, the implanted repair tissues were expected to increase in cellularity and possibly to generate other cartilage structural components. In order to follow the growth, OCT was exploited in the measurement of the homogeneity and the attenuation coefficient of the implanted material.

Immediately after the implantation, the structures of the four different tissue-engineered implants were readily recognized in both the OCT and ultrasound images and the filling of the defect could be well visualized from OCT images. Unfortunately, after two months of healing, there was practically no implanted material left in the implantation sites. The thin layer of tissue remaining in the damaged areas was assessed as being fibrocartilage. Thus, the sensitivity of OCT to detect the possible growth of articular cartilage could not be evaluated. However, OCT was found to be beneficial in the measurement of the remaining tissue thickness and in the evaluation of the integrity of cartilage surrounding the defect. OCT images showed that no significant wear or degeneration of the surrounding cartilage had occurred. Based on OCT and ultrasound images, it was assumed that the implanted repair materials had worn out away, and the PCL scaffolds used in the repair technique 4 were no longer in place. These speculations, however, will need to be verified with histological analysis at the end of the study.

7.6 CLINICAL POTENTIAL OF ARTHROSCOPIC OCT

Since light has a limited ability to penetrate in tissue, non-invasive OCT imaging of articular cartilage is not feasible. However, arthroscopic OCT imaging can be conducted during normal arthroscopy and it may not even require any additional arthroscopic portals.

The potential of arthroscopic OCT in clinical use is exciting. The strength of the technique lies in its high resolution, which is for example, superior to that of ultrasound imaging. Additionally, OCT permits a visualization of subsurface cartilage lesions, which are not revealed in conventional arthroscopy. As stated in this thesis and in previous studies, arthroscopic OCT provides a means to measure the thickness of cartilage up to 1.5-2.0 mm and thus it allows an evaluation of spontaneous or surgical cartilage repair, and makes it possible to estimate the degeneration and injuries of cartilage during conventional arthroscopic procedure.

The restricted light penetration limits its ability to assess thick human cartilage. The earliest signs of degeneration occur in the superficial zone. Therefore, the quantitative analysis of the tissue at depths exceeding 1.5 mm may not be as important as the analysis of the changes in the superficial zone. Light penetration could be improved by optical clearing [163–165]. This could help in the structural analysis of cartilage, but this would complicate the subsequent quantitative analysis, because optical clearing reduces light scattering within the tissue. The use of optical clearing of articular cartilage *in vivo* warrants for investigation.

Further development of the imaging probe and imaging geometry could simplify the imaging, and improve the quality of the images and their quantitative analysis. The use of sterilizable, multiuse probes would reduce the costs of the imaging per patient. OCT could also be combined with ultrasound imaging or complemented with other optical tissue analysis methods, such as near-infrared spectroscopy [166–168].

In addition to clinical use, OCT could be advantageously exploited in research into the causes of OA and in the cartilage injury treatment as it enables *in vivo* monitoring of the healing process.

8 Summary and conclusions

In this thesis, the feasibility of using OCT for imaging and in the quantitative analysis of articular cartilage was studied. The sensitivity of OCT to detect compositional and structural changes in articular cartilage was investigated by studying the OCT signals measured from agarose scaffolds with varying amount of cartilage structural components, and from equine articular cartilage. A measurement technique was developed utilizing simultaneous ultrasound and OCT imaging to assist in the arthroscopic determination of speed of sound in articular cartilage. Furthermore, the use of OCT in arthroscopic imaging of articular cartilage was tested in multiple human joints *in situ*. Finally, the potential of arthroscopic OCT for evaluation of the success of surgical cartilage repair was determined *in vivo* in an equine model.

The main conclusions may be summarized as follows:

- Compositional and structural changes in articular cartilage influence the OCT signal. However, the total attenuation and backscattering coefficients may not be sufficiently sensitive to detect the changes during degeneration, and the use of multivariate analysis of the OCT signal could be considered.
- Simultaneous ultrasound and OCT imaging allow a determination of speed of sound in cartilage during an arthroscopic examination. However, the measurement accuracy will need improvement before the technique can be used for the detection of cartilage degeneration.
- Arthroscopic OCT imaging of large and small human joints is feasible. OCT, as a complementary technique for conventional arthroscopy, improves the ability to detect and assess chondral lesions. Arthroscopic OCT has also value in the evaluation of the success of articular cartilage repair surgery and cartilage healing.

It is predicted that arthroscopic OCT imaging and the quantitative characterization of articular cartilage will have major clinical value in the assessment of degeneration and in the detection of injuries. OCT could have additional value in research when developing the novel cartilage treatment methods. It is likely that after optimization of the probe design, the benefits of utilizing an arthroscopic examination may well be improved even further.

Bibliography

[1] V. C. Mow, A. Ratcliffe, and A. R. Poole, "Cartilage and diarthrodial joints as paradigms for hierarchical materials and structures," *Biomaterials* **13,** 67–97 (1992).

[2] H. Forster and J. Fisher, "The influence of continuous sliding and subsequent surface wear on the friction of articular cartilage," *Proceedings of the Institution of Mechanical Engineers. Part H, Journal of engineering in medicine* **213,** 329–345 (1999).

[3] J. A. Buckwalter and J. Martin, "Degenerative joint disease," *Clinical symposia* **47,** 1–32 (1995).

[4] J. P. Arokoski, J. S. Jurvelin, U. Väätäinen, and H. J. Helminen, "Normal and pathological adaptations of articular cartilage to joint loading," *Scandinavian journal of medicine & science in sports* **10,** 186–198 (2000).

[5] J. A. Buckwalter and H. J. Mankin, "Articular cartilage. Part II: Degeneration and osteoarthrosis, repair, regeneration, and transplantation," *Journal of Bone and Joint Surgery - Series A* **79,** 612–632 (1997).

[6] R. C. Lawrence, D. T. Felson, C. G. Helmick, L. M. Arnold, H. Choi, R. A. Deyo, S. Gabriel, R. Hirsch, M. C. Hochberg, G. G. Hunder, J. M. Jordan, J. N. Katz, H. M. Kremers, and F. Wolfe, "Estimates of the prevalence of arthritis and other rheumatic conditions in the United States. Part II," *Arthritis & Rheumatism* **58,** 26–35 (2008).

[7] M. Blagojevic, C. Jinks, A. Jeffery, and K. P. Jordan, "Risk factors for onset of osteoarthritis of the knee in older adults: a systematic review and meta-analysis," *Osteoarthritis and Cartilage* **18,** 24–33 (2010).

[8] J. A. Buckwalter and T. D. Brown, "Joint injury, repair, and remodeling: roles in post-traumatic osteoarthritis," *Clinical orthopaedics and related research* **423,** 7–16 (2004).

[9] J. Borrelli, M. J. Silva, M. A. Zaegel, C. Franz, and L. J. Sandell, "Single high-energy impact load causes posttraumatic OA in young rabbits via a decrease in cellular metabolism," *Journal of Orthopaedic Research* **27,** 347–352 (2009).

[10] T. M. Simon and D. W. Jackson, "Articular cartilage: injury pathways and treatment options," *Sports medicine and arthroscopy review* **14,** 146–154 (2006).

[11] J. E. J. Bekkers, M. Inklaar, and D. B. F. Saris, "Treatment selection in articular cartilage lesions of the knee: a systematic review," *The American journal of sports medicine* **37 Suppl 1,** 148S–55S (2009).

[12] J. A. Buckwalter, D. D. Anderson, T. D. Brown, Y. Tochigi, and J. A. Martin, "The Roles of Mechanical Stresses in the Pathogenesis of Osteoarthritis: Implications for Treatment of Joint Injuries," *Cartilage* **4,** 286–294 (2013).

[13] S. Amin, M. P. LaValley, A. Guermazi, M. Grigoryan, D. J. Hunter, M. Clancy, J. Niu, D. R. Gale, and D. T. Felson, "The relationship between cartilage loss on magnetic resonance imaging and radiographic progression in men and women with knee osteoarthritis," *Arthritis and Rheumatism* **52,** 3152–3159 (2005).

[14] J. A. Carrino, A. Al Muhit, W. Zbijewski, G. K. Thawait, J. W. Stayman, N. Packard, R. Senn, D. Yang, D. H. Foos, J. Yorkston, and J. H. Siewerdsen, "Dedicated cone-beam CT system for extremity imaging," *Radiology* **270,** 816–24 (2014).

[15] H. Kokkonen, J. S. Suomalainen, A. Joukainen, H. Kröger, J. S. Sirola, J. Jurvelin, J. Salo, and J. Töyräs, "In vivo diagnostics of human knee cartilage lesions using delayed CBCT arthrography," *Journal of orthopaedic research* **32,** 403–12 (2014).

[16] G. E. Gold, C. A. Chen, S. Koo, B. A. Hargreaves, and N. K. Bangerter, "Recent advances in MRI of articular cartilage," *American Journal of Roentgenology* **193,** 628–638 (2009).

[17] M. J. Nissi, F. Toth, J. Zhang, S. Schmitter, M. Benson, C. S. Carlson, and J. M. Ellermann, "Susceptibility weighted imaging of cartilage canals in porcine epiphyseal growth cartilage ex vivo and in vivo," *Magnetic Resonance in Medicine* **71,** 2197–2205 (2014).

[18] B. H. Brismar, T. Wredmark, T. Movin, J. Leandersson, and O. Svensson, "Observer reliability in the arthroscopic classification of osteoarthritis of the knee," *The Journal of bone and joint surgery. British volume* **84,** 42–47 (2002).

[19] G. Spahn, H. M. Klinger, and G. O. Hofmann, "How valid is the arthroscopic diagnosis of cartilage lesions? Results of an opinion survey among highly experienced arthroscopic surgeons," *Archives of Orthopaedic and Trauma Surgery* **129,** 1117–1121 (2009).

[20] G. Spahn, H. M. Klinger, M. Baums, U. Pinkepank, and G. O. Hofmann, "Reliability in arthroscopic grading of cartilage lesions: Results of a prospective blinded study for evaluation of inter-observer reliability," *Archives of Orthopaedic and Trauma Surgery* **131,** 377–381 (2011).

[21] C. R. Chu, D. Lin, J. L. Geisler, C. T. Chu, F. H. Fu, and Y. Pan, "Arthroscopic microscopy of articular cartilage using optical coherence tomography," *The American journal of sports medicine* **32,** 699–709 (2004).

[22] N. C. R. te Moller, H. Brommer, J. Liukkonen, T. Virén, M. Timonen, P. H. Puhakka, J. S. Jurvelin, P. R. Van Weeren, and J. Töyräs, "Arthroscopic optical coherence tomography provides detailed information on articular cartilage lesions in horses," *Veterinary Journal* **197,** 589–595 (2013).

[23] W. Drexler, D. Stamper, C. Jesser, X. Li, C. Pitris, K. Saunders, S. Martin, M. B. Lodge, J. G. Fujimoto, and M. E. Brezinski, "Correlation of collagen organization with polarization sensitive imaging of in vitro cartilage: Implications for osteoarthritis," *Journal of Rheumatology* **28,** 1311–1318 (2001).

[24] C. Y. Xu, J. M. Schmitt, S. G. Carlier, and R. Virmani, "Characterization of atherosclerosis plaques by measuring both backscattering and attenuation coefficients in optical coherence tomography," *Journal of Biomedical Optics* **13** (2008).

[25] P. Cernohorsky, A. C. Kok, D. M. D. Bruin, M. J. Brandt, D. J. Faber, G. J. Tuijthof, G. M. Kerkhoffs, S. D. Strackee, and T. G. van Leeuwen, "Comparison of optical coherence tomography and histopathology in quantitative assessment of goat talus articular cartilage," *Acta orthopaedica* **86,** 257–263 (2015).

[26] Y. Pan, Z. Li, T. Xie, and C. R. Chu, "Hand-held arthroscopic optical coherence tomography for in vivo high-resolution imaging of articular cartilage," *Journal of biomedical optics* **8,** 648–654 (2003).

[27] J. A. Buckwalter and H. J. Mankin, "Articular cartilage. Part I: Tissue design and chondrocyte-matrix interactions," *Journal of Bone and Joint Surgery-American volume* **79A,** 600–611 (1997).

[28] J. P. Arokoski, M. M. Hyttinen, T. Lapveteläinen, P. Takács, B. Kosztáczky, L. Módis, V. Kovanen, and H. Helminen, "Decreased birefringence of the superficial zone collagen network in the canine knee (stifle) articular cartilage after long distance running training, detected by quantitative polarised light microscopy," *Annals of the rheumatic diseases* **55,** 253–264 (1996).

[29] V. C. Mow, M. H. Holmes, and W. M. Lai, "Fluid transport and mechanical properties of articular cartilage: a review," *Journal of biomechanics* **17,** 377–394 (1984).

[30] D. D. Anderson, S. Chubinskaya, F. Guilak, J. A. Martin, T. R. Oegema, S. A. Olson, and J. A. Buckwalter, "Post-traumatic osteoarthritis: Improved understanding and opportunities for early intervention," *Journal of Orthopaedic Research* **29,** 802–809 (2011).

[31] F. Nelson, R. C. Billinghurst, R. T. Pidoux, A. Reiner, M. Langworthy, M. McDermott, T. Malogne, D. F. Sitler, N. R. Kilambi, E. Lenczner, and A. R. Poole, "Early post-traumatic osteoarthritis-like changes in human articular cartilage following rupture of the anterior cruciate ligament," *Osteoarthritis and Cartilage* **14,** 114–119 (2006).

[32] N. Arden and M. C. Nevitt, "Osteoarthritis: Epidemiology," *Best Practice and Research: Clinical Rheumatology* **20,** 3–25 (2006).

[33] G. Peat, R. McCarney, and P. Croft, "Knee pain and osteoarthritis in older adults: a review of community burden and current use of primary health care," *Annals of the rheumatic diseases* **60,** 91–97 (2001).

[34] N. E. Lane and J. M. Thompson, "Management of osteoarthritis in the primary-care setting: an evidence-based approach to treatment," *The American journal of medicine* **103,** 25S–30S (1997).

[35] C. R. Denegar, D. R. Dougherty, J. E. Friedman, M. E. Schimizzi, J. E. Clark, B. A. Comstock, and W. J. Kraemer, "Preferences for heat, cold, or contrast in patients with knee osteoarthritis affect treatment response," *Clinical interventions in aging* **5,** 199–206 (2010).

[36] T. Schmalz, E. Knopf, H. Drewitz, and S. Blumentritt, "Analysis of biomechanical effectiveness of valgus-inducing knee brace for osteoarthritis of knee," *Journal of rehabilitation research and development* **47,** 419–429 (2010).

[37] A. W. S. Rutjes, P. Jüni, B. R. da Costa, S. Trelle, E. Nüesch, and S. Reichenbach, "Viscosupplementation for osteoarthritis of the knee: A systematic review and meta-analysis," *Annals of Internal Medicine* **157,** 180–191 (2012).

[38] E. Kon, G. Filardo, M. Drobnic, H. Madry, M. Jelic, N. van Dijk, and S. della Villa, "Non-surgical management of early knee osteoarthritis," *Knee Surgery, Sports Traumatology, Arthroscopy* **20,** 436–449 (2012).

[39] E. B. Hunziker, "Articular cartilage repair: Basic science and clinical progress. A review of the current status and prospects," *Osteoarthritis and Cartilage* **10,** 432–463 (2002).

[40] G. Knutsen, V. Isaksen, O. Johansen, L. Engebretsen, T. Ludvigsen, J. Drogset, S. E. Grøntvedt, T., T. Strand, and S. Roberts, "Autologous chondrocyte implantation compared with microfracture in the knee: A randomized trial," *The Journal of Bone and Joint Surgery* **86,** 455–464 (2004).

[41] R. Gudas, R. Kalesinskas, V. Kimtys, E. Stankevičius, V. Toliušis, G. Bernotavičius, and A. Smailys, "A prospective randomized clinical study of mosaic osteochondral autologous transplantation versus microfracture for the treatment of osteochondral defects in the knee joint in young athletes," *Arthroscopy - Journal of Arthroscopic and Related Surgery* **21,** 1066–1075 (2005).

[42] L. Kock, C. C. Van Donkelaar, and K. Ito, "Tissue engineering of functional articular cartilage: The current status," *Cell and Tissue Research* **347,** 613–627 (2012).

[43] J. R. Steadman, W. G. Rodkey, S. B. Singleton, and K. K. Briggs, "Microfracture technique forfull-thickness chondral defects: Technique and clinical results," *Operative Techniques in Orthopaedics* **7,** 300–304 (1997).

[44] M. Brittberg, A. Lindahl, A. Nilsson, C. Ohlsson, O. Isaksson, and L. Peterson, "Treatment of deep cartilage defects in the

knee with autologous chondrocyte transplantation," *The New England journal of medicine* **331,** 889–895 (1994).

[45] P. R. J. V. C. Boopalan, S. Sathishkumar, S. Kumar, and S. Chittaranjan, "Rabbit articular cartilage defects treated by allogenic chondrocyte transplantation," *International Orthopaedics* **30,** 357–361 (2006).

[46] A. Bedi, B. T. Feeley, and R. J. Williams, "Management of articular cartilage defects of the knee," *The Journal of bone and joint surgery. American volume* **92,** 994–1009 (2010).

[47] J. L. Favinger, A. S. Ha, M. E. Brage, and F. S. Chew, "Osteoarticular transplantation: recognizing expected postsurgical appearances and complications," *Radiographics* **35,** 780–92 (2015).

[48] E. B. Hunziker, K. Lippuner, M. J. B. Keel, and N. Shintani, "An educational review of cartilage repair: precepts & practice - myths & misconceptions - progress & prospects," *Osteoarthritis and cartilage* **23,** 334–50 (2015).

[49] T. A. E. Ahmed and M. T. Hincke, "Strategies for articular cartilage lesion repair and functional restoration," *Tissue engineering. Part B, Reviews* **16,** 305–329 (2010).

[50] S. Panseri, A. Russo, C. Cunha, A. Bondi, A. Di Martino, S. Patella, and E. Kon, "Osteochondral tissue engineering approaches for articular cartilage and subchondral bone regeneration," *Knee Surgery, Sports Traumatology, Arthroscopy* **20,** 1182–1191 (2012).

[51] F. T. Moutos, L. E. Freed, and F. Guilak, "A biomimetic three-dimensional woven composite scaffold for functional tissue engineering of cartilage," *Nature materials* **6,** 162–167 (2007).

[52] T. J. Klein, J. Malda, R. L. Sah, and D. W. Hutmacher, "Tissue engineering of articular cartilage with biomimetic zones," *Tissue engineering. Part B, Reviews* **15,** 143–157 (2009).

[53] E. A. Makris, J. C. Hu, and K. A. Athanasiou, "Hypoxia-induced collagen crosslinking as a mechanism for enhancing mechanical properties of engineered articular cartilage," *Osteoarthritis and Cartilage* **21,** 634–641 (2013).

[54] T. Boegård and K. Jonsson, "Radiography in osteoarthritis of the knee," *Skeletal Radiology* **28,** 605–615 (1999).

[55] A. W. Palmer, R. E. Guldberg, and M. E. Levenston, "Analysis of cartilage matrix fixed charge density and three-dimensional morphology via contrast-enhanced microcomputed tomography," *Proceedings of the National Academy of Sciences of the United States of America* **103,** 19255–19260 (2006).

[56] H. T. Kokkonen, J. S. Jurvelin, V. Tiitu, and J. Töyräs, "Detection of mechanical injury of articular cartilage using contrast enhanced computed tomography," *Osteoarthritis and cartilage* **19,** 295–301 (2011).

[57] A. Bashir, M. L. Gray, and D. Burstein, "Gd-DTPA2- as a measure of cartilage degradation," *Magnetic Resonance in Medicine* **36,** 665–673 (1996).

[58] Y. Xia, "Relaxation anisotropy in cartilage by NMR microscopy (μMRI) at 14-μm resolution," *Magnetic Resonance in Medicine* **39,** 941–949 (1998).

[59] M. J. Nissi, J. Töyräs, M. S. Laasanen, J. Rieppo, S. Saarakkala, R. Lappalainen, J. S. Jurvelin, and M. T. Nieminen, "Proteoglycan and collagen sensitive MRI evaluation of normal and degenerated articular cartilage," *Journal of Orthopaedic Research* **22,** 557–564 (2004).

[60] M. T. Nieminen, J. Rieppo, J. Töyräs, J. M. Hakumäki, J. Silvennoinen, M. M. Hyttinen, H. J. Helminen, and J. S. Jurvelin, "T2 relaxation reveals spatial collagen architecture in articular cartilage: A comparative quantitative MRI and polarized light microscopic study," *Magnetic Resonance in Medicine* **46,** 487–493 (2001).

[61] Y. Xia, J. B. Moody, and H. Alhadlaq, "Orientational dependence of T2 relaxation in articular cartilage: A microscopic MRI (μMRI) study," *Magnetic Resonance in Medicine* **48,** 460–469 (2002).

[62] C. Liess, S. Lüsse, N. Karger, M. Heller, and C. G. Glüer, "Detection of changes in cartilage water content using MRI T2-mapping in vivo," *Osteoarthritis and Cartilage* **10,** 907–913 (2002).

[63] A. Bashir, M. L. Gray, J. Hartke, and D. Burstein, "Nondestructive imaging of human cartilage glycosaminoglycan concentration by MRI," *Magnetic Resonance in Medicine* **41,** 857–865 (1999).

[64] S. L. Gold, A. J. Burge, and H. G. Potter, "MRI of hip cartilage: Joint morphology, structure, and composition," *Clinical Orthopaedics and Related Research* **470,** 3321–3331 (2012).

[65] M. Brittberg, "Evaluation of cartilage injuries and cartilage repair," *Osteologie* **9,** 17–25 (2000).

[66] K. Hattori, Y. Takakura, M. Ishimura, T. Habata, K. Uematsu, and K. Ikeuch, "Quantitative arthroscopic ultrasound evaluation of living human cartilage," *Clinical Biomechanics* **19,** 213–216 (2004).

[67] E. Kaleva, T. Virén, S. Saarakkala, J. Sahlman, J. Sirola, J. Puhakka, T. Paatela, H. Kröger, I. Kiviranta, J. S. Jurvelin, and J. Töyräs, "Arthroscopic Ultrasound Assessment of Articular Cartilage in the Human Knee Joint: A Potential Diagnostic Method," *Cartilage* **2,** 246–253 (2011).

[68] E. Kaleva, S. Saarakkala, J. S. Jurvelin, T. Virén, and J. Töyräs, "Effects of Ultrasound Beam Angle and Surface Roughness on the Quantitative Ultrasound Parameters of Articular Cartilage," *Ultrasound in Medicine and Biology* **35,** 1344–1351 (2009).

[69] T. Virén, S. Saarakkala, V. Tiitu, J. Puhakka, I. Kiviranta, J. S. Jurvelin, and J. Töyräs, "Ultrasound evaluation of mechanical injury of bovine knee articular cartilage under arthroscopic control," *IEEE Transactions on Ultrasonics, Ferroelectrics, and Frequency Control* **58,** 148–155 (2011).

[70] E. Chérin, A. Saed, P. Laugier, P. Netter, and G. Berger, "Evaluation of acoustical parameter sensitivity to age-related and osteoarthritic changes in articular cartilage using 50-MHZ ultrasound," *Ultrasound in Medicine and Biology* **24,** 341–354 (1998).

[71] J. Töyräs, J. Rieppo, M. T. Nieminen, H. J. Helminen, and J. S. Jurvelin, "Characterization of enzymatically induced degradation of articular cartilage using high frequency ultrasound," *Physics in medicine and biology* **44,** 2723–2733 (1999).

[72] J. Töyräs, M. S. Laasanen, S. Saarakkala, M. J. Lammi, J. Rieppo, J. Kurkijärvi, R. Lappalainen, and J. S. Jurvelin, "Speed of sound in normal and degenerated bovine articular cartilage," *Ultrasound in Medicine and Biology* **29,** 447–454 (2003).

[73] G. A. Joiner, E. R. Bogoch, K. P. Pritzker, M. D. Buschmann, A. Chevrier, and F. S. Foster, "High frequency acoustic parameters of human and bovine articular cartilage following experimentally-induced matrix degradation," *Ultrasonic imaging* **23,** 106–116 (2001).

[74] D. Huang, E. A. Swanson, C. P. Lin, J. S. Schuman, W. G. Stinson, W. Chang, M. R. Hee, T. Flotte, K. Gregory, C. A. Puliafito, T. Flotire, K. Gregory, C. A. Puliafito, and J. G. Fujimoto, "Optical coherence tomography," *Science* **254,** 1178–1181 (1991).

[75] W. Drexler and J. G. Fujimoto, "State-of-the-art retinal optical coherence tomography," *Progress in Retinal and Eye Research* **27,** 45–88 (2008).

[76] S. Marschall, B. Sander, M. Mogensen, T. M. Jørgensen, and P. E. Andersen, "Optical coherence tomography-current technology and applications in clinical and biomedical research," *Analytical and Bioanalytical Chemistry* **400,** 2699–2720 (2011).

[77] J. S. Schuman, T. Pedut-Kloizman, E. Hertzmark, M. R. Hee, J. R. Wilkins, J. G. Coker, C. A. Puliafito, J. G. Fujimoto, and E. A. Swanson, "Reproducibility of nerve fiber layer thickness measurements using optical coherence tomography," *Ophthalmology* **103,** 1889–1898 (1996).

[78] H. Yabushita, B. E. Bouma, S. L. Houser, H. T. Aretz, I. K. Jang, K. H. Schlendorf, C. R. Kauffman, M. Shishkov, D. H. Kang, E. F. Halpern, and G. J. Tearney, "Characterization of human atherosclerosis by optical coherence tomography," *Circulation* **106,** 1640–1645 (2002).

[79] G. J. Tearney, E. Regar, T. Akasaka, T. Adriaenssens, P. Barlis, H. G. Bezerra, B. Bouma, N. Bruining, J. M. Cho, S. Chowdhary, et al., "Consensus standards for acquisition, measurement, and reporting of intravascular optical coherence tomography studies: A report from the International Working Group for Intravascular Optical Coherence Tomography Standardization and Validation," *Journal of the American College of Cardiology* **59,** 1058–1072 (2012).

[80] T. Gambichler, V. Jaedicke, and S. Terras, "Optical coherence tomography in dermatology: Technical and clinical aspects," *Archives of Dermatological Research* **303,** 457–473 (2011).

[81] J. Izatt, H.-W. W. H.-W. Wang, M. Kulkarni, M. Canto, and M. Sivak, "Optical coherence microscopy in gastrointestinal tissues," *Summaries of papers presented at the Conference on Lasers and Electro-Optics* **2,** 1017–1028 (1996).

[82] E. Alarousu, L. Krehut, T. Prykäri, and R. Myllylä, "Study on the use of optical coherence tomography in measurements

of paper properties," *Measurement Science and Technology* **16,** 1131–1137 (2005).

[83] S. Zhong, Y. C. Shen, L. Ho, R. K. May, J. A. Zeitler, M. Evans, P. F. Taday, M. Pepper, T. Rades, K. C. Gordon, R. Mller, and P. Kleinebudde, "Non-destructive quantification of pharmaceutical tablet coatings using terahertz pulsed imaging and optical coherence tomography," *Optics and Lasers in Engineering* **49,** 361–365 (2011).

[84] Y. Pan, R. Birngruber, J. Rosperich, and R. Engelhardt, "Low-coherence optical tomography in turbid tissue: theoretical analysis," *Applied optics* **34,** 6564–6574 (1995).

[85] A. F. Fercher, W. Drexler, C. K. Hitzenberger, and T. Lasser, "Optical coherence tomography - principles and applications," *Reports on Progress in Physics* **66,** 239–303 (2003).

[86] J. M. Schmitt, "Optical Coherence Tomography (OCT): a review," *IEEE Journal on Selected Topics in Quantum Electronics* **5,** 1205–1215 (1999).

[87] A. Fercher, C. Hitzenberger, G. Kamp, and S. El-Zaiat, "Measurement of intraocular distances by backscattering spectral interferometry," *Optics Communications* **117,** 43–48 (1995).

[88] G. Häusler and M. Lindner, ""Coherence Radar" and "Spectral Radar" - New Tools for Dermatological Diagnosis," *Journal of Biomedical Optics* **3,** 21 (1998).

[89] R. Leitgeb, C. Hitzenberger, and A. Fercher, "Performance of fourier domain vs. time domain optical coherence tomography," *Optics express* **11,** 889–894 (2003).

[90] M. Choma, M. Sarunic, C. Yang, and J. Izatt, "Sensitivity advantage of swept source and Fourier domain optical coherence tomography," *Optics express* **11,** 2183–2189 (2003).

[91] W. Drexler and J. G. Fujimoto, *Optical Coherence Tomography*, First ed. (Springer Berlin Heidelberg, Berlin, Heidelberg, 2008).

[92] A. F. Fercher, "Optical coherence tomography - development, principles, applications," *Zeitschrift fur medizinische Physik* **20,** 251–276 (2010).

[93] M. E. Brezinski, *Optical coherence tomography: Principles and applications*, First ed. (Academic Press, London, UK, 2006).

[94] E. Hecht, *Optics*, Fourth ed. (Addison Wesley, San Francisco, 2002).

[95] J. A. Izatt, M. R. Hee, G. M. Owen, E. A. Swanson, and J. G. Fujimoto, "Optical coherence microscopy in scattering media," *Optics letters* **19,** 590–592 (1994).

[96] T. Niemelä, T. Virén, J. Liukkonen, D. Argüelles, N. C. R. te Moller, P. H. Puhakka, J. S. Jurvelin, R.-M. Tulamo, and J. Töyräs, "Application of optical coherence tomography enhances reproducibility of arthroscopic evaluation of equine joints," *Acta veterinaria Scandinavica* **56,** 1–8 (2014).

[97] C. R. Chu, N. J. Izzo, J. J. Irrgang, M. Ferretti, and R. K. Studer, "Clinical diagnosis of potentially treatable early articular cartilage degeneration using optical coherence tomography," *Journal of biomedical optics* **12,** 051703 (2007).

[98] C. R. Chu, A. Williams, D. Tolliver, C. K. Kwoh, S. Bruno, and J. J. Irrgang, "Clinical optical coherence tomography of early articular cartilage degeneration in patients with degenerative meniscal tears," *Arthritis and Rheumatism* **62,** 1412–1420 (2010).

[99] K. Zheng, S. D. Martin, C. H. Rashidifard, B. Liu, and M. E. Brezinski, "In vivo micron-scale arthroscopic imaging of human knee osteoarthritis with optical coherence tomography:

comparison with magnetic resonance imaging and arthroscopy," *American journal of orthopedics* **39,** 122–125 (2010).

[100] P. Cernohorsky, D. M. de Bruin, M. van Herk, J. Bras, D. J. Faber, S. D. Strackee, and T. G. van Leeuwen, "In-situ imaging of articular cartilage of the first carpometacarpal joint using co-registered optical coherence tomography and computed tomography," *Journal of Biomedical Optics* **17,** 060501 (2012).

[101] M. J. Roberts, S. B. Adams, N. A. Patel, D. L. Stamper, M. S. Westmore, S. D. Martin, J. G. Fujimoto, and M. E. Brezinski, "A new approach for assessing early osteoarthritis in the rat," *Analytical and Bioanalytical Chemistry* **377,** 1003–1006 (2003).

[102] X. Li, S. Martin, C. Pitris, R. Ghanta, D. L. Stamper, M. Harman, J. G. Fujimoto, and M. E. Brezinski, "High-resolution optical coherence tomographic imaging of osteoarthritic cartilage during open knee surgery," *Arthritis Research & Therapy* **7,** R318–23 (2005).

[103] S. Saarakkala, S.-Z. Wang, Y.-P. Huang, and Y.-P. Zheng, "Quantification of the optical surface reflection and surface roughness of articular cartilage using optical coherence tomography," *Physics in medicine and biology* **54,** 6837–6852 (2009).

[104] T. Virén, Y. P. Huang, S. Saarakkala, H. Pulkkinen, V. Tiitu, A. Linjama, I. Kiviranta, M. J. Lammi, A. Brünott, H. Brommer, R. Van Weeren, P. A. J. Brama, Y. P. Zheng, J. S. Jurvelin, and J. Töyräs, "Comparison of ultrasound and optical coherence tomography techniques for evaluation of integrity of spontaneously repaired horse cartilage," *Journal of Medical Engineering & Technology* **36,** 185–192 (2012).

[105] N. A. Patel, J. Zoeller, D. L. Stamper, J. G. Fujimoto, and M. E. Brezinski, "Monitoring osteoarthritis in the rat model using optical coherence tomography," *IEEE transactions on medical imaging* **24,** 155–159 (2005).

[106] S. B. Adams, P. R. Herz, D. L. Stamper, M. J. Roberts, S. Bourquin, N. A. Patel, K. Schneider, S. D. Martin, S. Shortkroff, J. G. Fujimoto, and M. E. Brezinski, "High-resolution imaging of progressive articular cartilage degeneration," *Journal of orthopaedic research* **24,** 708–715 (2006).

[107] D. M. Bear, M. Szczodry, S. Kramer, C. H. Coyle, P. Smolinski, and C. R. Chu, "Optical coherence tomography detection of subclinical traumatic cartilage injury," *Journal of orthopaedic trauma* **24,** 577–582 (2010).

[108] Y. E. Yarker, R. M. Aspden, and D. W. Hukins, "Birefringence of articular cartilage and the distribution on collagen fibril orientations," *Connective tissue research* **11,** 207–213 (1983).

[109] T. Xie, S. Guo, J. Zhang, Z. Chen, and G. M. Peavy, "Use of polarization-sensitive optical coherence tomography to determine the directional polarization sensitivity of articular cartilage and meniscus," *Journal of biomedical optics* **11,** 064001 (2006).

[110] J. J. Shyu, C. H. Chan, M. W. Hsiung, P. N. Yang, H. W. Chen, and W. C. Kuo, "Polarization Sensitive Optical Coherence Tomography and the Extracted Optical Properties," *Progress In Electromagnetics Research* **91,** 365–376 (2009).

[111] S. Jiao and L. V. Wang, "Jones-matrix imaging of biological tissues with quadruple-channel optical coherence tomography," *Journal of biomedical optics* **7,** 350–358 (2002).

[112] C. W. Han, C. R. Chu, N. Adachi, A. Usas, F. H. Fu, J. Huard, and Y. Pan, "Analysis of rabbit articular cartilage repair after chondrocyte implantation using optical coherence tomography," *Osteoarthritis and cartilage* **11,** 111–121 (2003).

[113] S.-Z. Wang, Y.-P. Huang, Q. Wang, Y.-P. Zheng, and Y.-H. He, "Assessment of depth and degeneration dependences of articular cartilage refractive index using optical coherence tomography in vitro," *Connective tissue research* **51,** 36–47 (2010).

[114] R. P. Silverman, D. Passaretti, W. Huang, M. A. Randolph, and M. J. Yaremchuk, "Injectable tissue-engineered cartilage using a fibrin glue polymer," *Plastic and reconstructive surgery* **103,** 1809–1818 (1999).

[115] W. Schuurman, P. A. Levett, M. W. Pot, P. R. van Weeren, W. J. A. Dhert, D. W. Hutmacher, F. P. W. Melchels, T. J. Klein, and J. Malda, "Gelatin-methacrylamide hydrogels as potential biomaterials for fabrication of tissue-engineered cartilage constructs," *Macromolecular Bioscience* **13,** 551–561 (2013).

[116] P. A. Levett, F. P. W. Melchels, K. Schrobback, D. W. Hutmacher, J. Malda, and T. J. Klein, "A biomimetic extracellular matrix for cartilage tissue engineering centered on photocurable gelatin, hyaluronic acid and chondroitin sulfate," *Acta Biomaterialia* **10,** 214–223 (2014).

[117] J. Visser, F. P. W. Melchels, J. E. Jeon, E. M. van Bussel, L. S. Kimpton, H. M. Byrne, W. J. A. Dhert, P. D. Dalton, D. W. Hutmacher, and J. Malda, "Reinforcement of hydrogels using three-dimensionally printed microfibres," *Nature communications* **6,** 6933 (2015).

[118] L. P. Li, J. Soulhat, M. D. Buschmann, and A. Shirazi-Adl, "Nonlinear analysis of cartilage in unconfined ramp compression using a fibril reinforced poroelastic model," *Clinical Biomechanics* **14,** 673–682 (1999).

[119] R. K. Korhonen, M. S. Laasanen, J. Töyräs, R. Lappalainen, H. J. Helminen, and J. S. Jurvelin, "Fibril reinforced poroelastic model predicts specifically mechanical behavior of normal, proteoglycan depleted and collagen degraded articular cartilage," *Journal of Biomechanics* **36,** 1373–1379 (2003).

[120] W. Wilson, C. C. Van Donkelaar, B. Van Rietbergen, K. Ito, and R. Huiskes, "Stresses in the local collagen network of articular cartilage: A poroviscoelastic fibril-reinforced finite element study," *Journal of Biomechanics* **37,** 357–366 (2004).

[121] P. Julkunen, P. Kiviranta, W. Wilson, J. S. Jurvelin, and R. K. Korhonen, "Characterization of articular cartilage by combining microscopic analysis with a fibril-reinforced finite-element model," *Journal of Biomechanics* **40,** 1862–1870 (2007).

[122] J. T. A. Mäkelä, M. R. J. Huttu, and R. K. Korhonen, "Structure-function relationships in osteoarthritic human hip joint articular cartilage," *Osteoarthritis and Cartilage* **20,** 1268–1277 (2012).

[123] K. A. M. Kulmala, H. J. Pulkkinen, L. Rieppo, V. Tiitu, I. Kiviranta, A. Brünott, H. Brommer, R. van Weeren, P. A. J. Brama, M. T. Mikkola, R. K. Korhonen, J. S. Jurvelin, and J. Töyräs, "Contrast-Enhanced Micro-Computed Tomography in Evaluation of Spontaneous Repair of Equine Cartilage," *Cartilage* **3,** 235–244 (2012).

[124] H. E. Panula, M. M. Hyttinen, J. P. Arokoski, T. K. Lå ngsjö, A. Pelttari, I. Kiviranta, and H. J. Helminen, "Articular cartilage superficial zone collagen birefringence reduced and cartilage thickness increased before surface fibrillation in experimental osteoarthritis," *Annals of the rheumatic diseases* **57,** 237–245 (1998).

[125] H. J. Mankin, H. Dorfman, L. Lippiello, and A. Zarins, "Biochemical and metabolic abnormalities in articular cartilage from osteo-arthritic human hips. II. Correlation of morphology with biochemical and metabolic data," *The Journal of bone and joint surgery. American volume* **53,** 523–537 (1971).

[126] M. G. Ehrlich, P. A. Houle, G. Vigliani, and H. J. Mankin, "Correlation between articular cartilage collagenase activity and osteoarthritis," *Arthritis and rheumatism* **21,** 761–766 (1978).

[127] I. Kiviranta, J. Jurvelin, A. M. Säämänen, and H. J. Helminen, "Microspectrophotometric quantitation of glycosamino-

glycans in articular cartilage sections stained with Safranin O," *Histochemistry* **82,** 249–255 (1985).

[128] N. P. Camacho, P. West, P. A. Torzilli, and R. Mendelsohn, "FTIR microscopic imaging of collagen and proteoglycan in bovine cartilage," *Biopolymers - Biospectroscopy Section* **62,** 1–8 (2001).

[129] A. Boskey and N. Pleshko Camacho, "FT-IR imaging of native and tissue-engineered bone and cartilage," *Biomaterials* **28,** 2465–2478 (2007).

[130] L. Rieppo, S. Saarakkala, T. Närhi, H. J. Helminen, J. S. Jurvelin, and J. Rieppo, "Application of second derivative spectroscopy for increasing molecular specificity of fourier transform infrared spectroscopic imaging of articular cartilage," *Osteoarthritis and Cartilage* **20,** 451–459 (2012).

[131] D. H. Goldstein, *Polarized Light*, Third ed. (CRC Press, Boca Raton, 2010).

[132] J. Rieppo, J. Hallikainen, J. S. Jurvelin, I. Kiviranta, H. J. Helminen, and M. M. Hyttinen, "Practical considerations in the use of polarized light microscopy in the analysis of the collagen network in articular cartilage," *Microscopy Research and Technique* **71,** 279–287 (2008).

[133] D. Faber, F. van der Meer, M. Aalders, and T. van Leeuwen, "Quantitative measurement of attenuation coefficients of weakly scattering media using optical coherence tomography," *Optics express* **12,** 4353–4365 (2004).

[134] T. G. van Leeuwen, D. J. Faber, and M. C. Aalders, "Measurement of the axial point spread function in scattering media using single-mode fiber-based optical coherence tomography," *IEEE Journal of Selected Topics in Quantum Electronics* **9,** 227–233 (2003).

[135] J. M. Schmitt, A. Knüttel, and R. F. Bonner, "Measurement of optical properties of biological tissues by low-coherence reflectometry," *Applied optics* **32,** 6032–6042 (1993).

[136] V. E. Modest, M. C. Murphy, and R. W. Mann, "Optical verification of a technique for in situ ultrasonic measurement of articular cartilage thickness," *Journal of biomechanics* **22,** 171–176 (1989).

[137] S. Wold, M. Sjöström, and L. Eriksson, "PLS-regression: a basic tool of chemometrics," *Chemometrics and Intelligent Laboratory Systems* **58,** 109–130 (2001).

[138] A. Lorber and B. R. Kowalski, "Alternatives to cross-validatory estimation of the number of factors in multivariate calibration," *Applied Spectroscopy* **44,** 1464–1470 (1990).

[139] N. C. R. te Moller, H. Brommer, J. Liukkonen, T. Virén, M. Timonen, P. H. Puhakka, J. S. Jurvelin, P. R. Van Weeren, and J. Töyräs, "Arthroscopic optical coherence tomography provides detailed information on articular cartilage lesions in horses," *Veterinary Journal* **197,** 589–595 (2013).

[140] F. de Bont, N. Brill, R. Schmitt, M. Tingart, B. Rath, T. Pufe, H. Jahr, and S. Nebelung, "Evaluation of Single-Impact-Induced Cartilage Degeneration by Optical Coherence Tomography," *BioMed research international* **2015,** 486794 (2015).

[141] J. Welzel, M. Bruhns, and H. H. Wolff, "Optical coherence tomography in contact dermatitis and psoriasis," *Archives of Dermatological Research* **295,** 50–55 (2003).

[142] D. P. Popescu, M. G. Sowa, M. D. Hewko, and L.-P. Choo-Smith, "Assessment of early demineralization in teeth using the signal attenuation in optical coherence tomography images," *Journal of biomedical optics* **13,** 054053 (2008).

[143] Q. Zhao, "Ex vivo determination of glucose permeability and optical attenuation coefficient in normal and adenomatous

human colon tissues using spectral domain optical coherence tomography," *Journal of Biomedical Optics* **17,** 105004 (2012).

[144] F. J. Van Der Meer, D. J. Faber, D. M. B. Sassoon, M. C. Aalders, G. Pasterkamp, and T. G. Van Leeuwen, "Localized measurement of optical attenuation coefficients of atherosclerotic plaque constituents by quantitative optical coherence tomography," *IEEE Transactions on Medical Imaging* **24,** 1369–1376 (2005).

[145] G. van Soest, T. Goderie, E. Regar, S. Koljenović, G. L. J. H. van Leenders, N. Gonzalo, S. van Noorden, T. Okamura, B. E. Bouma, G. J. Tearney, J. W. Oosterhuis, P. W. Serruys, and A. F. W. van der Steen, "Atherosclerotic tissue characterization in vivo by optical coherence tomography attenuation imaging," *Journal of biomedical optics* **15,** 011105 (2010).

[146] J. Kalkman, A. V. Bykov, D. J. Faber, and T. G. van Leeuwen, "Multiple and dependent scattering effects in Doppler optical coherence tomography," *Optics express* **18,** 3883–3892 (2010).

[147] P. Lee, W. Gao, and X. Zhang, "Performance of single-scattering model versus multiple-scattering model in the determination of optical properties of biological tissue with optical coherence tomography," *Applied optics* **49,** 3538–3544 (2010).

[148] S. Nebelung, U. Marx, N. Brill, D. Arbab, V. Quack, H. Jahr, M. Tingart, B. Zhou, M. Stoffel, R. Schmitt, and B. Rath, "Morphometric grading of osteoarthritis by optical coherence tomography–an ex vivo study," *Journal of orthopaedic research* **32,** 1381–8 (2014).

[149] T. Xie, S. Guo, J. Zhang, Z. Chen, and G. M. Peavy, "Determination of characteristics of degenerative joint disease using optical coherence tomography and polarization sensitive optical coherence tomography," *Lasers in Surgery and Medicine* **38,** 852–865 (2006).

[150] J. Martel-Pelletier, C. Boileau, J. P. Pelletier, and P. J. Roughley, "Cartilage in normal and osteoarthritis conditions," *Best Practice and Research: Clinical Rheumatology* **22,** 351–384 (2008).

[151] J. T. A. Mäkelä, Z. S. Rezaeian, S. Mikkonen, R. Madden, S. K. Han, J. S. Jurvelin, W. Herzog, and R. K. Korhonen, "Site-dependent changes in structure and function of lapine articular cartilage 4 weeks after anterior cruciate ligament transection," *Osteoarthritis and Cartilage* **22,** 869–878 (2014).

[152] R. Ortmann, "Use of polarized light for quantitative determination of the adjustment of the tangential fibres in articular cartilage," *Anatomy and embryology* **148,** 109–120 (1975).

[153] D. P. Speer and L. Dahners, "The collagenous architecture of articular cartilage. Correlation of scanning electron microscopy and polarized light microscopy observations," *Clinical orthopaedics and related research* **139,** 267–275 (1979).

[154] J. Rogowska, C. M. Bryant, and M. E. Brezinski, "Cartilage thickness measurements from optical coherence tomography," *Journal of the Optical Society of America. A, Optics, image science, and vision* **20,** 357–367 (2003).

[155] J. G. Fujimoto, M. E. Brezinski, G. J. Tearney, S. A. Boppart, B. Bouma, M. R. Hee, J. F. Southern, and E. A. Swanson, "Optical biopsy and imaging using optical coherence tomography," *Nature medicine* **1,** 970–972 (1995).

[156] S. L. Myers, K. Dines, D. A. Brandt, K. D. Brandt, and M. E. Albrecht, "Experimental Assessment by High-Frequency Ultrasound of Articular-Cartilage Thickness and Osteoarthritic Changes," *The Journal of rheumatology* **22,** 109–116 (1995).

[157] J. K. F. Suh, I. Youn, and F. H. Fu, "An in situ calibration of an ultrasound transducer: A potential application for an ultrasonic indentation test of articular cartilage," *Journal of Biomechanics* **34,** 1347–1353 (2001).

[158] J. Töyräs, M. S. Laasanen, S. Saarakkala, M. J. Lammi, J. Rieppo, J. Kurkijärvi, R. Lappalainen, and J. S. Jurvelin, "Speed of sound in normal and degenerated bovine articular cartilage," *Ultrasound in Medicine and Biology* **29,** 447–454 (2003).

[159] T. Aoki, N. Nitta, and A. Furukawa, "Non-invasive speed of sound measurement in cartilage by use of combined magnetic resonance imaging and ultrasound: An initial study," *Radiological Physics and Technology* **6,** 480–485 (2013).

[160] H. Brommer, M. S. Laasanen, P. A. J. Brama, P. R. van Weeren, A. Barneveld, H. J. Helminen, and J. S. Jurvelin, "Influence of age, site, and degenerative state on the speed of sound in equine articular cartilage," *American Journal of Veterinary Research* **66,** 1175–1180 (2005).

[161] S. Patil, Y. Zheng, J. Wu, and J. Shi, "Measurement of depth-dependence and anisotropy of ultrasound speed of bovine articular cartilage in vitro," *Ultrasound in Medicine and Biology* **30,** 953–963 (2004).

[162] K. Eder, R. Schmitt, and R. Müller-Rath, "Imaging of artificial cartilage with optical coherence tomography," *Progress in Biomedical Optics and Imaging - Proceedings of SPIE* **6858,** 68580J (2008).

[163] V. V. Tuchin, I. L. Maksimova, D. A. Zimnyakov, I. L. Kon, A. H. Mavlutov, and A. A. Mishin, "Light propagation in tissues with controlled optical properties," *Journal of Biomedical Optics* **2,** 401 (1997).

[164] C. P. Neu, T. Novak, K. F. Gilliland, P. Marshall, and S. Calve, "Optical clearing in collagen- and proteoglycan-rich osteochondral tissues," *Osteoarthritis and cartilage* **23,** 405–13 (2015).

[165] A. Bykov, T. Hautala, M. Kinnunen, A. Popov, S. Karhula, S. Saarakkala, M. T. Nieminen, V. Tuchin, and I. Meglinski,

"Imaging of subchondral bone by optical coherence tomography upon optical clearing of articular cartilage," *Journal of biophotonics* (2015).

[166] J. K. Marticke, A. Hösselbarth, K. L. Hoffmeier, I. Marintschev, S. Otto, M. Lange, H. K. W. Plettenberg, G. Spahn, and G. O. Hofmann, "How do visual, spectroscopic and biomechanical changes of cartilage correlate in osteoarthritic knee joints?," *Clinical Biomechanics* **25,** 332–340 (2010).

[167] I. Afara, I. Prasadam, R. Crawford, Y. Xiao, and A. Oloyede, "Non-destructive evaluation of articular cartilage defects using near-infrared (NIR) spectroscopy in osteoarthritic rat models and its direct relation to Mankin score," *Osteoarthritis and Cartilage* **20,** 1367–1373 (2012).

[168] M. V. Padalkar, R. G. Spencer, and N. Pleshko, "Near infrared spectroscopic evaluation of water in hyaline cartilage," *Annals of Biomedical Engineering* **41,** 2426–2436 (2013).

PIA PUHAKKA

Prior to surgical treatment, the severity and extent of articular cartilage lesions are evaluated arthroscopically. However, conventional arthroscopy is unable to reveal subsurface lesions, the true depth of the defect, and early stage tissue degeneration. In this thesis, novel methods were investigated to apply optical coherence tomography to qualitative and quantitative evaluation of articular cartilage degeneration and success of the repair surgeries. Optical coherence tomography, as a complementary to conventional arthroscopy, could improve the arthroscopic assessment of articular cartilage, treatment planning and treatment follow-up.

UNIVERSITY OF
EASTERN FINLAND

uef.fi

**PUBLICATIONS OF
THE UNIVERSITY OF EASTERN FINLAND**
Dissertations in Forestry and Natural Sciences

ISBN 978-952-61-2019-5
ISSN 1798-5668